UNCLASSIFIED

AD 268 393

Reproduced
by the

ARMED SERVICES TECHNICAL INFORMATION AGENCY
ARLINGTON HALL STATION
ARLINGTON 12, VIRGINIA

UNCLASSIFIED

NOTICE: When government or other drawings, specifications or other data are used for any purpose other than in connection with a definitely related government procurement operation, the U. S. Government thereby incurs no responsibility, nor any obligation whatsoever; and the fact that the Government may have formulated, furnished, or in any way supplied the said drawings, specifications, or other data is not to be regarded by implication or otherwise as in any manner licensing the holder or any other person or corporation, or conveying any rights or permission to manufacture, use or sell any patented invention that may in any way be related thereto.

62-1-5
XEROX

DA 36-039 SC-87475

EDL-E58

CATALOGED BY ASTIA
AS AD NO. 268393

Elementary Results for High Frequency Scattering by Cones

J. E. BURKE, L. MOWER, AND V. TWERSKY

THEOR

SYLVANIA ELECTRONIC SYSTEMS
Government Systems Management
for GENERAL TELEPHONE & ELECTRONICS

ELECTRONIC DEFENSE LABORATORIES

ELECTRONIC DEFENSE LABORATORIES

P. O. Box 205

Mountain View, California

ENGINEERING REPORT

EDL-E58
April 24, 1961

ELEMENTARY RESULTS FOR HIGH FREQUENCY SCATTERING BY CONES

by

J. E. Burke, L. Mower, and V. Twersky

Prepared for the U. S. Army Signal Research and Development Laboratory under Signal Corps Contract DA 36-039 SC-87475.

Approved for publication . . . . . Victor Twersky
Head of Research

SYLVANIA ELECTRIC PRODUCTS INC.

ELEMENTARY RESULTS FOR HIGH FREQUENCY SCATTERING BY CONES

by

J. E. Burke, L. Mower, and V. Twersky

Sylvania Electronic Defense Laboratories, Mountain View, California

CONTENTS

Page

ABSTRACT 1

1. INTRODUCTION 1

2. SCALAR FIELDS 2

2.1. Scattering by an Arbitrary Object 2
2.2. Scattering by a Finite Cone. 6
2.3. Elementary Considerations. 18

3. ELECTROMAGNETIC FIELDS. 21

4. NUMERICAL ILLUSTRATIONS. 23

REFERENCES. 40

ILLUSTRATIONS

Figure	Title	Page
1	Scattering geometry.	3
2	The geometry for scattering by a finite cone.	7
3	Comparison of $\|I(2x)\|^2$ of the text with the Frauhnofer aperture factors for the strip, $(\sin x/x)^2$, and the disk $(2J_1(x)/x)^2$	14
4	Scattering at the specular angle	19
5	Traces of some specular beams on the plane $z = 1$ for $\Gamma = 10.5^\circ$ and $\theta_0 < \pi/2$; the angular and radial coordinates are respectively φ and $\tan\theta$.	24
6	Traces of some specular beams on the plane $z = -1$ for $\Gamma = 10.5^\circ$ and $\theta_0 > \pi/2$; the angular and radial coordinates are respectively φ and $\tan\theta$.	25
7	The variation of $\cos\theta_0 - \cos\theta$ on the beams of Figure 5; the angular and radial coordinates are respectively φ and $\cos\theta_0 - \cos\theta$.	26
8	The variation of $\cos\theta_0 - \cos\theta$ on the beams of Figure 6; the angular and radial coordinates are respectively φ and $\cos\theta_0 - \cos\theta$.	27
9	Half power values of θ on specular beams as a function of Γ and θ_0.	28
10	Half power values of φ on specular beams as a function of Γ and θ_0.	29
11	$\sigma_\pm$, and $\sigma(s)\|I\|^2$, for $\theta_0 = 0$ and $\varphi = 0$; here and on the following graphs, the dashed curve represents $\sigma(s)\|I\|^2$.	30
12	σ_l and $\sigma(s)\|I\|^2$, for $\theta_0 = 0$ and $\varphi = 0$.	31
13	σ_d for $\theta_0 = 0$ and $\varphi = 0$.	32
14	$\sigma_\pm$ and $\sigma(s)\|I\|^2$, for $\theta_0 = 42^\circ$ and $\varphi = 0$.	34

ILLUSTRATIONS (Con't)

Figure	Title	Page
15	σ_{ℓ} and $\sigma(s)\|I\|^2$, for $\theta_o = 42^o$ and $\varphi = 0$.	35
16	σ_{ℓ} for $\theta_o = 42^o$ and $\varphi = 0$.	36
17	$\sigma_{\pm}$ and $\sigma(s)\|I\|^2$ for $\theta_o = \pi - 42^o$, and $\varphi = 0, \pi$.	37
18	σ_{ℓ} and $\sigma(s)\|I\|^2$ for $\theta_o = \pi - 42^o$, and $\varphi = 0, \pi$.	38
19	σ_{ℓ} for $\theta_o = \pi - 42^o$ and $\varphi = 0, \pi$.	39

ELEMENTARY RESULTS FOR HIGH FREQUENCY SCATTERING BY CONES

by

J. E. Burke, L. Mower, and V. Twersky

Sylvania Electronic Defense Laboratories, Mountain View, California

ABSTRACT

Elementary high frequency results for scattering by finite cones are obtained by approximating the surface fields in the integral representation by their geometrical optics values. Both singly and doubly truncated cones are considered. A general expression is obtained for the location of the "specular beam" (i.e., the surface generated by the geometrically reflected rays), and simple results for the field on and off the "beam" are developed. In particular, it is shown that for many practical purposes a universal curve exists for the scattering pattern. This curve, which depends on a parameter involving the cone's length and half angle, falls more or less between the Fraunhofer "aperture" patterns for the strip and disk, and differs essentially in that the minima are not zero. Numerical illustrations are given.

1. INTRODUCTION

The scattering of waves by finite cones whose length and base dimensions are large compared to wavelength ("high frequency scattering range") is of interest to various physical and engineering applications. In this range we obtain elementary approximations from the surface integral representation of the scattered field (scalar or vector) by replacing the unknown surface fields by their geometrical optics values, and then evaluating the integral.

The limitations of this type of approximation are well known; however, such results, particularly in the vicinity of the "principal scattered lobe", have been shown to be adequate for many practical applications. Better approximations for the fields in other directions may be obtained by the methods of Fock, Keller, Siegel, and others[1] who use essentially more complete representations for the surface fields.

In the following, we begin with the general scalar problem of scattering by an arbitrary totally reflecting object, and specialize the result to far-field scattering by the cone. We then treat the corresponding vector electromagnetic problem. The physical significance of the results are discussed, and numerical illustrations are given.

It is to be stressed that the approximations in this report are based on well known elementary procedures, and that some of the results are to be found elsewhere[2, 3]. However, our final results differ from those derived by others on the basis of the same initial approximation (because of differing treatments of certain integrals that arise) and are more detailed than those we presented previously.[3]

2. SCALAR FIELDS

2.1. Scattering by an Arbitrary Object

The scalar scattering problem of a point source exciting an arbitrary totally reflecting object may be formulated as follows: In the volume external to the scatterer (whose surface is specified by S), we require a solution of

$$(1) \qquad (\nabla^2 + k^2)\psi(\underset{\sim}{r}, \underset{\sim}{r}_t) = \delta(|\underset{\sim}{r} - \underset{\sim}{r}_t|), \quad \nabla^2 = \partial_x^2 + \partial_y^2 + \partial_z^2, \quad k = 2\pi/\lambda,$$

subject to prescribed boundary conditions at the surface of the scatterer. (The delta function indicates a source at $\underset{\sim}{r} = \underset{\sim}{r}_t$; see Figure 1 for the scattering geometry.) The solution is to be of the form

$$(2) \qquad \psi(\underset{\sim}{r}, \underset{\sim}{r}_t) = \psi_o(\underset{\sim}{r}, \underset{\sim}{r}_t) + u(\underset{\sim}{r}, \underset{\sim}{r}_t), \quad \psi_o(\underset{\sim}{r}, \underset{\sim}{r}_t) = \frac{e^{ikR_t}}{4\pi R_t}, \quad R_t = |\underset{\sim}{r} - \underset{\sim}{r}_t|,$$

where ψ_o represents the incident field, and where the associated scattered field fulfills

$$(3) \qquad u(\underset{\sim}{r}, \underset{\sim}{r}_t) \sim \left[\frac{e^{ikr_t}}{4\pi r_t}\right]\left[\frac{e^{ikr}}{r}\right] g(\hat{r}, \hat{r}_t), \quad \text{as } r_t \to \infty \quad \text{and} \quad r \to \infty.$$

The "scattering amplitude" $g(\hat{r}, \hat{r}_t)$ indicates the "far-field" response

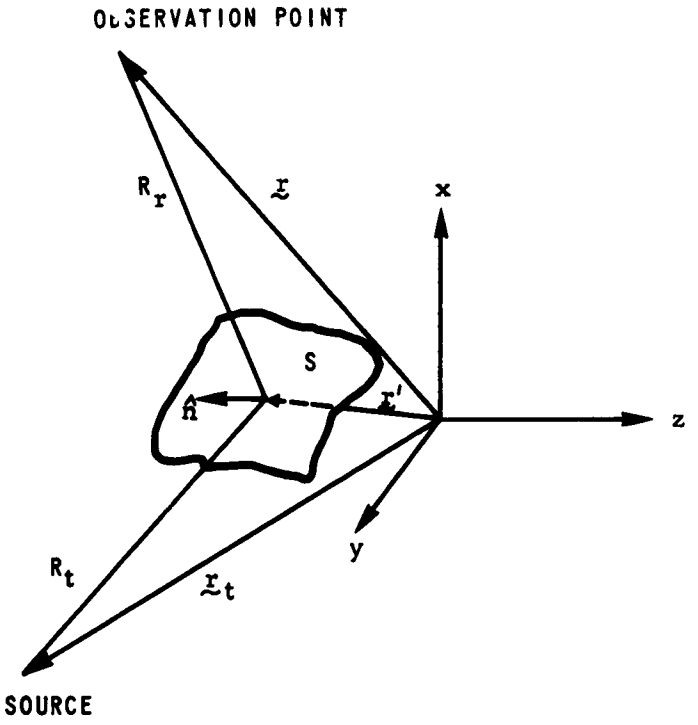

Figure 1. Scattering geometry.

in the direction $\hat{r} = \underset{\sim}{r}/r$ arising from plane wave excitation of direction $-\hat{r}_t$ (i.e., a source at $\underset{\sim}{r}_t \to \hat{r}_t \infty$). The corresponding received power is given by

$$P_r = \frac{P_t G A \sigma}{(4\pi R_t R_r)^2}, \qquad \sigma = 4\pi |g|^2, \tag{4}$$

where P_t is the power of the source, G is its gain, A is the area of the receiving aperture, and σ is the normalized differential ("bistatic") scattering cross section.

In general, we may represent u rigorously as an integral over the scatterer's surface; thus

$$u(\underset{\sim}{r}, \underset{\sim}{r}_t) = \int_S [\mathcal{G}(|\underset{\sim}{r}-\underset{\sim}{r}'|)\partial_n \psi(\underset{\sim}{r}', \underset{\sim}{r}_t) - \psi(\underset{\sim}{r}', \underset{\sim}{r}_t)\partial_n \mathcal{G}(|\underset{\sim}{r}-\underset{\sim}{r}'|)]\, dS, \tag{5}$$

where $\mathcal{G}(|\underset{\sim}{r}-\underset{\sim}{r}'|) \equiv \mathcal{G}(R_r) = -e^{ikR_r}/4\pi R_r$ is the free space scalar Green's function, and $\hat{n}$ is the outward normal to the surface. Consequently, were the surface fields ψ and $\partial_n \psi$ known, then u (and g) would follow on integration.

In the high frequency range we obtain approximations for u and g by replacing the unknown surface fields in (5) by their geometrical optics values; i.e., we use the surface fields which would exist on an infinite plane tangent to the point in question. If the total field is to vanish at the scatterer, we insert in (5) the boundary condition $\psi = 0$, and the geometric value

$$\begin{aligned} \partial_n \psi &= 2\partial_n \psi_0 \quad \text{on lit side} \\ &= 0 \qquad \text{on dark side} \end{aligned} \tag{6}$$

where the "lit" and "dark"portions of the scatterer's surface are taken in the sense of geometrical optics. Thus we obtain

$$u \approx 2\int_L \mathcal{G}\partial_n \psi_0\, dS \equiv u_- \; ; \tag{7}$$

here, and in subsequent equations, the integration is restricted to the lit portion of S unless specified otherwise. Similarly for vanishing normal derivative, we insert in (5) the boundary condition $\partial_n \psi = 0$, and the geometric value

$$\begin{aligned} \psi &= 2\psi_0 \quad \text{on lit side} \\ &= 0 \qquad \text{on dark side}, \end{aligned} \tag{8}$$

to obtain

$$u \approx -2\int_L \psi_o \partial_n \mathcal{G}\, dS \equiv u_+ . \tag{9}$$

Substituting the explicit forms of $\mathcal{G}$ and ψ_o into (7) and (9) leads to

$$\begin{Bmatrix} u_- \\ u_+ \end{Bmatrix} \approx \pm \frac{2ik}{(4\pi)^2}\int_L \frac{e^{ik(R_r+R_t)}}{R_r R_t}\begin{Bmatrix} \hat{n}\cdot\hat{R}_t \\ \hat{n}\cdot\hat{R}_r \end{Bmatrix} dS, \tag{10}$$

where we have neglected the higher powers of $1/R_r$ and $1/R_t$.

The scattered fields (10) may be split into "reflected" and "shadow forming" field components[4]; the "reflected" field, u_L, essentially governs geometrical reflections, while the "shadow forming" field, u_D, is most significant near the forward direction (e.g., it interferes with the incident field near the scatterer to produce the geometrical shadow). To obtain this alternate representation we initially use the decomposition (2) in (5), and note that the integral involving ψ_o vanishes identically. Then, in the remaining integral, we replace u and $\partial_n u$ by their values consistent with the boundary conditions, and the approximations (6) and (8); thus we obtain

$$u_\pm = \pm u_L + u_D, \quad u_{\frac{L}{D}} = \frac{-ik}{(4\pi)^2}\int_{\frac{L}{D}} \frac{e^{ik(R_t+R_r)}}{R_t R_r}\hat{n}\cdot(\hat{R}_t \pm \hat{R}_r)\, dS, \tag{10'}$$

where L and D denote respectively the lit and dark side of the scatterer. As a consequence of Green's theorem, u_D of (10') is equivalent to an integral over any surface which together with D encloses a volume free of sources. In particular u_D may be expressed as an integral over L and combined with u_L to obtain (10).

The scattering amplitudes associated with (10) are

$$g_\pm = \frac{-ik}{2\pi}\int_L e^{ik(\hat{\nu}-\hat{r})\cdot r'}\beta_\pm\, dS, \quad \beta_+ = \hat{n}\cdot\hat{r}, \quad \beta_- = \hat{n}\cdot\hat{\nu}, \quad \hat{\nu} = -\hat{r}_t, \tag{11}$$

or, equivalently,

$$g_\pm = \pm g_L + g_D, \quad g_{\frac{L}{D}} = \frac{ik}{2\pi}\int_{\frac{L}{D}} e^{ikr'\cdot(\hat{\nu}-\hat{r})}\beta_{\frac{L}{D}}(\varphi')\, dS, \quad \beta_{\frac{L}{D}} = \frac{\beta_- \mp \beta_+}{2}. \tag{11'}$$

The corresponding total scattering cross section may be obtained from the forward amplitude scattering theorem:

$$(12)\quad Q(\hat{\nu}) = \oint |g(\hat{r},\hat{\nu})|^2 d\Omega_r = \frac{4\pi}{k}\mathrm{Im}\, g(\hat{\nu},\hat{\nu}) \approx \frac{4\pi}{k}\mathrm{Im}\, g_D(\hat{\nu},\hat{\nu}) = 2\int_D [-\hat{n}\cdot\hat{\nu}]\, dS;$$

thus, to the present approximation the total scattering cross section for either boundary condition equals twice the scatterer's projection on a plane perpendicular to $\hat{\nu}$ (i.e., twice the area of the shadow).

2.2 Scattering by a Finite Cone

In this section we specialize (11) to treat singly and doubly truncated cones.

Consider a finite right circular cone of half angle Γ, with slant height ℓ and base radius a, whose vertex is at the origin of a rectangular coordinate system, and whose axis coincides with the positive z axis; see Figure 2. The remaining coordinate axes are chosen so that $\hat{\nu}$ lies in the xz plane, i.e.,

$$(13)\quad \hat{\nu} = -\hat{x}\sin\theta_0 + \hat{z}\cos\theta_0, \quad 0 \le \theta_0 \le \pi.$$

Then the vectors in (12), expressed in the usual spherical coordinates, are given explicitly by

$$\hat{r} = \hat{x}\cos\varphi\sin\theta + \hat{y}\sin\varphi\sin\theta + \hat{z}\cos\theta,$$

$$(14)\quad \hat{r}' = \hat{x}\cos\varphi'\sin\Gamma + \hat{y}\sin\varphi'\sin\Gamma + \hat{z}\cos\Gamma,$$

$$\hat{n} = \hat{x}\cos\varphi'\cos\Gamma + \hat{y}\sin\varphi'\cos\Gamma - \hat{z}\sin\Gamma,$$

where the above forms for $\hat{r}'$ and $\hat{n}$ apply for a point on the convex part of the cone; on the base, which we assume to be flat, $r' = r'\sin\theta'(\hat{x}\cos\varphi' + \hat{y}\sin\varphi') + \ell\cos\Gamma\hat{z}$, and $\hat{n} = \hat{z}$.

In terms of

$$A = \sin\theta_0 + \cos\varphi\sin\theta, \quad B = \sin\varphi\sin\theta, \quad D = \sqrt{A^2+B^2},$$

$$(15)$$

$$P = \cot\Gamma(\cos\theta_0 - \cos\theta), \quad \cos\varphi_s = \frac{A}{D}, \quad \sin\varphi_s = \frac{B}{D},$$

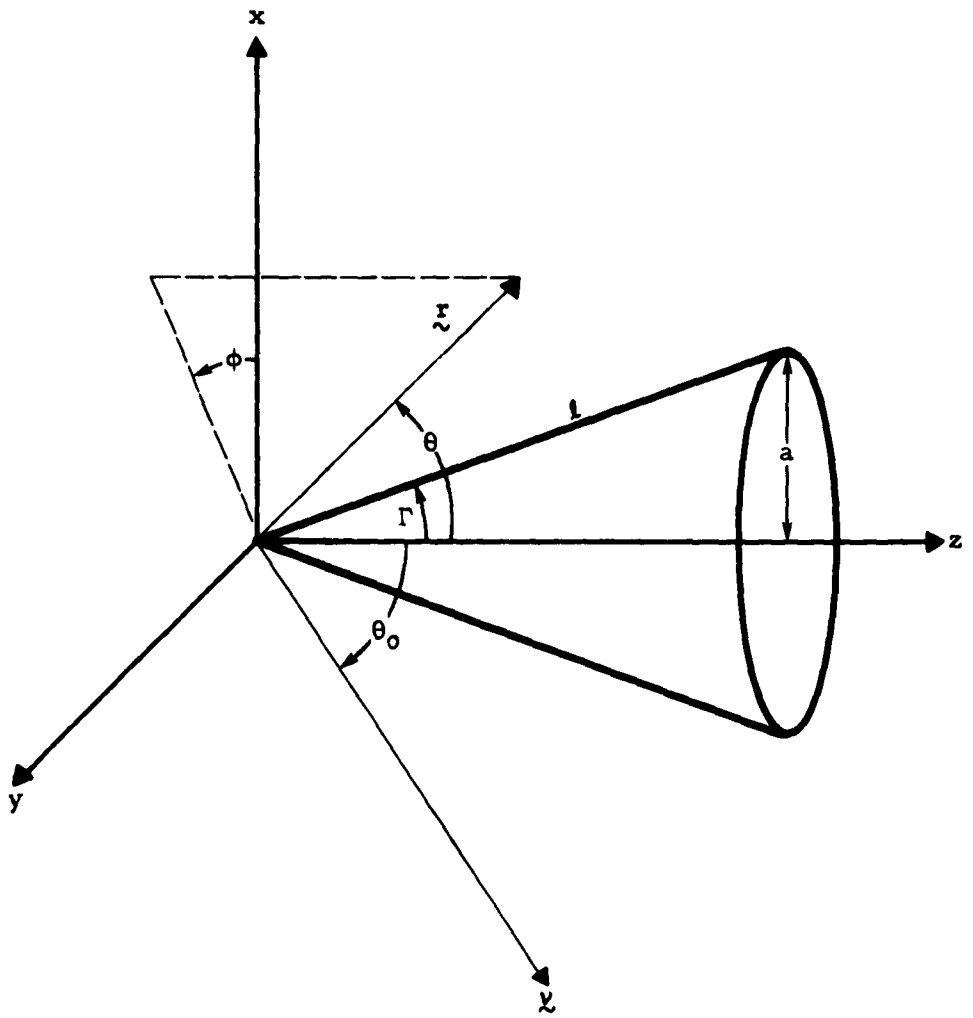

Figure 2. The geometry for scattering by a finite cone.

the contribution to (11) arising from integrating over a portion of the convex surface of the cone is given by

$$C_{\pm}(\hat{r},\hat{\nu}) = \frac{-ik\sin\Gamma}{2\pi}\int_0^{a\csc\Gamma} r' e^{ikr'P\sin\Gamma} F_{\pm}(r';k)\,dr', \tag{16}$$

where

$$F_{\pm} = \int_{-\varphi_i}^{\varphi_i} e^{-ikr'D\sin\Gamma\cos(\varphi'-\varphi_s)} \beta_{\pm}(\varphi')\,d\varphi',$$

$$\beta_- = -\sin\theta_0\cos\Gamma\cos\varphi' - \cos\theta_0\sin\Gamma, \tag{17}$$

$$\beta_+ = \cos\Gamma\sin\theta\cos(\varphi'-\varphi) - \sin\Gamma\cos\theta\,.$$

The limits of integration $\pm\varphi_i$, corresponding to the cone generators (the "shadow boundaries") along which $\hat{\nu}\cdot\hat{n} = 0$, are defined by

$$\cos\varphi_i = -\cot\theta_0\tan\Gamma. \tag{18}$$

Thus the convex surface is totally illuminated for $0 \le \theta_0 \le \Gamma$ $(\varphi_i = \pi)$, partially illuminated for $\Gamma < \theta_0 < \pi-\Gamma$, and "dark" for $\theta_0 > \pi - \Gamma$ $(\varphi_i = 0)$. When $\theta_0 > \pi/2$ the base of the cone is also "lit" and the resulting contribution to $g_{\pm}$ is the amplitude for a circular disk:

$$B_{\pm}(\hat{r},\hat{\nu}) = \frac{-ika^2}{2} e^{ikaP}\left[\frac{2J_1(kaD)}{kaD}\right]\frac{[\cos\theta + \cos\theta_0 \pm (\cos\theta - \cos\theta_0)]}{2}; \tag{19}$$

see Silver[5] for a detailed analysis of the circular "aperture factor". Combining (16) and (19) (and omitting the subscripts) we have

$$g(\hat{r},\hat{\nu}) = \begin{cases} C(\hat{r},\hat{\nu}), & 0 \le \theta_0 < \pi/2 \\ C(\hat{r},\hat{\nu}) + B(\hat{r},\hat{\nu}), & \pi/2 < \theta_0 \le \pi - \Gamma \\ B(\hat{r},\hat{\nu}), & \pi - \Gamma < \theta_0 \le \pi \end{cases} \tag{20}$$

or equivalently

$$g(\hat{r},\hat{\nu}) = C(\hat{r},\hat{\nu})H(0 \le \theta_0 \le \pi-\Gamma) + B(\hat{r},\hat{\nu})H\left(\tfrac{\pi}{2} < \theta_0 \le \pi\right) \equiv CH_1 + BH_2\,, \tag{20'}$$

where the step function H is unity in the range indicated in its argument and zero elsewhere.

In general, for arbitrary directions of incidence and observation, we cannot evaluate C exactly. However, when $D = 0$, the factor F is independent of r', and (16) is given by a product of elementary integrals. We shall consider this special case first and then the general case. Subsequently we extend our results to treat doubly truncated cones, and show how our results are related to those obtained by geometrical optics procedures.

Special case, $D = 0$: From equation (15) it follows that D is zero when

$$\hat{r} = \hat{\nu}, \qquad r = \hat{\mu} \equiv -\hat{x}\sin\theta_0 - \hat{z}\cos\theta_0, \tag{21}$$

i.e., for observation in the forward direction ($\varphi = \pi, \theta = \theta_0$), and in the direction corresponding to the reflection of $\hat{\nu}$ in the xy plane ($\varphi = \pi, \theta = \pi - \theta_0$; for example, back scattering for axial incidence). The resulting values of F are

$$\begin{aligned} F_- &= -2(\sin\theta_0\cos\Gamma\sin\varphi_i + \varphi_i\cos\theta_0\sin\Gamma), \\ F_+ &= -2(\sin\theta\cos\Gamma\sin\varphi_i + \varphi_i\cos\theta\sin\Gamma), \end{aligned} \tag{22}$$

where in F_+, $\theta = \theta_0$ for $\hat{r} = \hat{\nu}$, and $\theta = \pi - \theta_0$ for $\hat{r} = \hat{\mu}$.

Thus in the forward direction the form (21') reduces to

$$g(\hat{\nu},\hat{\nu}) = \frac{ika^2}{2\pi}\left\{\left[\varphi_i\cos\theta_0 + \cot\Gamma\sin\theta_0\sin\varphi_i\right]H_1 + \pi|\cos\theta_0|H_2\right\}. \tag{23}$$

The total scattering cross section as given by (12) may be written in the form

$$Q(\hat{\nu}) = 2a^2\left\{\cot\Gamma\sin\theta_0\sin^3\varphi_i H_1 + \tfrac{1}{2}(2\varphi_i - \sin 2\varphi_i)\cos\theta_0 H_1 + \pi|\cos\theta_0|H_2\right\}. \tag{24}$$

The first term of (24) is the total scattering cross section for the isosceles triangle defined by the shadow boundaries; the base and leg of this triangle are $2a\sin\varphi_i$ and $a\csc\Gamma$ respectively. The remaining terms together give the total scattering cross section for the larger segment of the base cut by the chord joining the shadow boundaries. In particular if $\varphi_i = 0$ $(\pi - \Gamma \le \theta_0 \le \pi)$ or if $\varphi_i = \pi$ $(0 \le \theta_0 \le \Gamma)$, then $Q = 2\pi a^2|\cos\theta_0|$ as for a disk of radius a. On the other hand if $\varphi_i = \pi/2$ $(\theta_0 = \pi/2)$, then $Q = 2a^2\cot\Gamma$ as for the triangle of base $2a$ and height $a\cot\Gamma$.

For the second case of (21) we obtain

$$(25)\quad g_{\pm}(\hat{\mu},\hat{\nu}) = \frac{\varphi_i\cos\theta_0 \mp \cot\Gamma\sin\theta_0\sin\varphi_i}{\pi\cos^2\theta_0}\left\{\frac{\pm i\tan^2\Gamma}{2}\left[ikh\cos\theta_0 e^{2ikh\cos\theta_0} + \frac{1-e^{2ikh\cos\theta_0}}{2k}\right]\right\}H_1 \pm \frac{ika^2}{2}\cos\theta_0 e^{2ikh\cos\theta_0}H_2,$$

where $h = a\cot\Gamma$. The term in curly brackets is the back scattering amplitude for nose on incidence on a cone of half angle Γ and height $h\cos\theta_0$; e.g., for axial incidence on the present cone,[2]

$$(26)\quad g_{\pm}(-\hat{z},\hat{z}) = \pm i\frac{\tan^2\Gamma}{2}\left[ikhe^{2ikh} + \frac{1-e^{2ikh}}{2k}\right].$$

In (25) and (26) the term which is not proportional to k is a base edge contribution. (In general an edge field is proportional to $1/\sqrt{k}$, but in the present case there is an additional factor of $\sqrt{k}$ since we are on the "caustic" of the edge field[8].) The term of order $1/k$ is a tip contribution. The term proportional to k corresponds to specular reflection by the base.

In the range $\theta_0 \le \pi/2$, we have $H_1 = 1$ and $H_2 = 0$. The two cases corresponding to $kh\cos\theta_0 \to 0$ are contained in (23). Thus in the limit $\Gamma \to \frac{\pi}{2}\ (h \to 0)$, (25) reduces to the required disk result:

$$(27)\quad \lim_{\Gamma\to\pi/2} g_{\pm}(\hat{\mu},\hat{\nu}) = \mp\frac{ika^2\cos\theta_0}{2}.$$

Similarly for $\theta_0 \to \pi/2$, we obtain the forward scattered value for a triangular plate:

$$(28)\quad \lim_{\theta_0\to\pi/2} g_{\pm}(\hat{\mu},\hat{\nu}) = g_{\pm}(\hat{x},\hat{x}) = \frac{ika^2\cot\Gamma}{2\pi}.$$

At the other limit $kh\cos\theta_0 >> 1$, $\theta_0 < \pi/2$ the base edge term dominates and (25), and (26) are given approximately by

$$(29)\quad \begin{aligned} g_{\pm}(\hat{\mu},\hat{\nu}) &\approx \frac{-ia\tan\Gamma}{2\pi\cos\theta_0} e^{2ikh\cos\theta_0}(\cot\Gamma\sin\theta_0\sin\varphi_0 \mp \varphi_i\cos\theta_0), \\ g_{\mp}(-\hat{z},\hat{z}) &\approx \pm\frac{ia\tan\Gamma e^{2ikh}}{2}. \end{aligned}$$

These forms are included primarily to facilitate comparison with the results of more rigorous procedures based essentially on better approximations than

geometrical optics for the surface field at the cone's edge. The reader is referred to Siegel's[6,7] analysis of back scattering for nose-on-incidence based on approximating the edge field in the integral representation by means of Sommerfeld's solution for the infinite wedge, and to Keller's[8,9] analysis which uses the asymptotic form of Sommerfeld's solution to obtain the appropriate diffraction coefficients for the "edge rays". The leading term of Keller's result is given by[8]

$$(30)\quad 4\pi\left|g_{\mp}(-\hat{z},\hat{z})\right|^2 = \frac{4\pi^3 a^2}{(3\pi+\Gamma)^2}\cot^2\left(\frac{4\pi^2}{3\pi+2\Gamma}\right)\left(\mp 1+\frac{\cos\frac{2\pi^2}{3\pi+2\Gamma}-\cos\frac{6\pi^2}{3\pi+2\Gamma}}{\cos\frac{2\pi^2}{3\pi+2\Gamma}-1}\right)^2,$$

which corresponds to incident rays single-diffracted by the cone's edge; compare with the rough approximation obtained from (29):

$$(31)\quad 4\pi\left|g_{\mp}(-\hat{z},\hat{z})\right|^2 = \frac{a^2\tan^2\Gamma}{4}.$$

Keller also derives the doubly-diffracted edge rays (which are excited by the singly-diffracted rays traveling across the "back" of the cone), etc. Siegel has prepared a detailed compilation of microwave measurements on back scattering versus ka and has shown that Keller's first two orders of diffracted rays give results for the intensity maxima in accord with experiment.

General case: In general we approximate F of (17) for large k by the method of stationary phase; this result is then substituted into (16) and the final integration performed to obtain C. Physically speaking, for a given direction of observation, the stationary phase procedure picks out the generator (or generators) of the cone which contributes most significantly to the scattered field. The r' integration provides the appropriate weighted sum of the contributions from each point on the generator.

The phase in (17) is stationary for those values of φ' satisfying

$$(32)\quad \left(\frac{\partial\mathcal{L}'}{\partial\varphi'}\right)\cdot(\hat{v}-\hat{r}) = r'\sin\Gamma D\sin(\varphi'-\varphi_s) = 0,$$

i.e., for $\varphi' = \varphi_s, \pi+\varphi_s$. There are three possibilities corresponding to different ranges of θ_o:

$$(33)\quad \begin{aligned} &\pi/2 < \theta_o \le \pi-\Gamma, && \pi/2 > \varphi_i \ge 0,\\ &\Gamma < \theta_o \le \pi/2, && \pi > \varphi_i \ge \pi/2,\\ &0 < \theta_o \le \Gamma, && \varphi_i = \pi. \end{aligned}$$

In the first range there is at most one stationary point; in the second, at least one and possibly two; in the last range there are always two. Keeping the two stationary points explicit, the usual stationary phase procedure applied to (17) gives

$$F(r',k) = \sqrt{\frac{2\pi}{kr'D\sin\Gamma}}\left\{\beta(\varphi_s)e^{-ikr'D\sin\Gamma+i\frac{\pi}{4}} + \beta(\pi+\varphi_s)e^{ikr'D\sin\Gamma-i\frac{\pi}{4}}\right\}. \tag{34}$$

When the cone is totally illuminated the stationary phase procedure need not be used. For this case $\varphi_i = \pi$ and (17) may be evaluated exactly in terms of Bessel functions:

$$F(r',k) = \pi\left\{\left[\beta(\varphi_s)+\beta(\pi+\varphi_s)\right]J_0(kr'D\sin\Gamma) + i\left[\beta(\varphi_s)-\beta(\pi+\varphi_s)\right]J_1(kr'D\sin\Gamma)\right\}, \tag{35}$$

$$0 \le \theta_o \le \Gamma.$$

When $kD >> 1$ we replace the Bessel functions by their asymptotic forms

$$J_n(t) \sim \sqrt{\frac{2}{\pi t}}\cos\left(t - \frac{n\pi}{2} - \frac{\pi}{4}\right), \quad t >> 1, \tag{36}$$

and obtain (34).

The stationary phase procedure cannot be applied when D is near zero (i. e., for observation near the special directions considered previously). For this range we expand the exponential factor of (17) in powers of D and integrate term by term. For total illumination the required result follows from (35) by using the origin forms of the Bessel functions:

$$J_n(t) = \frac{1}{n!}\left(\frac{t}{2}\right)^n\left[1 - \left(\frac{t}{2}\right)^2\frac{1}{n+1} + \cdots\right], \quad t << 1. \tag{37}$$

In the following we discount this range of D and use (34).

Substituting (34) into (16) we write C in the form

$$C(\hat{r},\hat{\nu}) = \left(\frac{2}{3}\right)\sqrt{\frac{ka}{2\pi D}}\,\ell e^{-i\pi/4}\left\{\beta(\varphi_s)\,I\left[ka(P-D)\right] - i\beta(\pi+\varphi_s)\,I\left[ka(P+D)\right]\right\}, \tag{38}$$

$$I[x] = \frac{3}{2}\int_0^1 \sqrt{t}\,e^{ixt}dt = \frac{3}{2ix}\left\{e^{ix} - \frac{1}{2}\int_0^1 \frac{e^{ixt}}{\sqrt{t}}\,dt\right\},$$

where the last integral in essentially the complex Fresnel integral.

The limiting forms of $I[x]$ are

$$I[x] \sim 1 + i\frac{3}{5}x - \frac{x^2 3}{14} + \cdots, \quad x \to 0; \tag{39}$$

$$I[x] \sim \left(\frac{3}{2}\right)\frac{e^{ix}}{ix} - \frac{3}{4x}\sqrt{\frac{\pi}{ix}} + \frac{3}{4x^2}e^{ix} + \cdots, \quad x \to \infty, \tag{40}$$

The analytical behavior of C is determined primarily by the I-integrals (which vary much more rapidly with θ and φ than do their multipliers). The graph of $|I(2x)|^2$ for a generator of length ℓ falls more or less between the Fraunhofer patterns for the disk of diameter ℓ and the strip of width ℓ. As can be seen from Figure 3 the essentially different feature of the present "pattern factor" is that the minima are not zero. Near the principal maximum the intensities for the disk, cone, and strip factors are respectively $1-0.25x^2$, $1-0.274x^2$, $1-0.333x^2$.

When $ka(P \pm D) >> 1$ we use the asymptotic form (40) in (38) and obtain

$$C(\hat{r},\hat{v}) \sim -\ell e^{ikaP}\sqrt{\frac{i}{2\pi kaD}}\left[\frac{\beta(\varphi_s)e^{-ikaD}}{P-D} - \frac{i\beta(\pi+\varphi_s)e^{ikaD}}{P+D}\right]. \tag{41}$$

An alternate procedure for obtaining this result is to first carry out the r' integration in (16). This leads to

$$C(\hat{r},\hat{v}) = \frac{-ika}{2\pi}\int_{-\varphi_i}^{\varphi_i}\beta(\varphi')\left\{\frac{e^{ika[P-D\cos(\varphi'-\varphi_s)]}}{ika\sin\Gamma[P-D\cos(\varphi'-\varphi_s)]} - \frac{1-e^{ika[P-D\cos(\varphi'-\varphi_s)]}}{[ika\sin\Gamma(P-D\cos(\varphi'-\varphi_s)]^2}\right\}d\varphi'.$$

For the present case $(D \neq P)$ the first term of the expression dominates. Dropping the second, and evaluating the first by the method of stationary phase we again obtain (41).

The special directions for which $P = D$ correspond to values of θ and φ satisfying

$$\sqrt{\sin^2\theta_0 + \sin^2\theta + 2\cos\varphi\sin\theta\sin\theta_0} = \cot\Gamma(\cos\theta_0 - \cos\theta), \quad \theta_0 < \theta. \tag{42}$$

These are the directions of specular reflection, and their envelope defines the "specular beam". Thus (41) applies off the specular beam . On the other hand, for observation on or "near" the "beam", such that $ka(P-D) << 1$

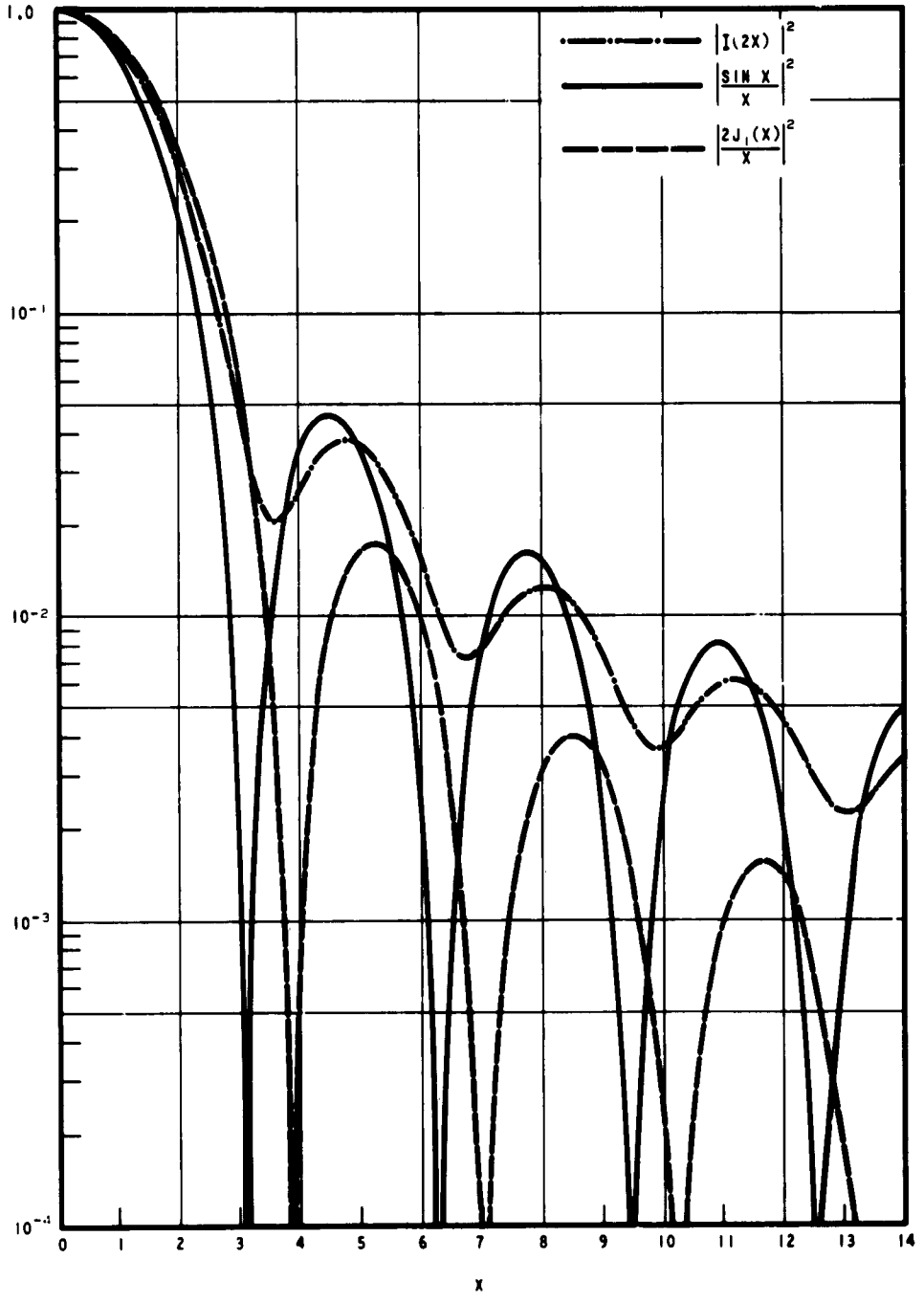

Figure 3. Comparison of $|I(2x)|^2$ for the cone with the Fraunhofer pattern factors for the strip $(\sin x/x)^2$, and for the disk $(2J_1(x)/x)^2$; here the length of the cone's generator, the strip width, and the disk's diameter are all equal.

and $ka(P+D) >> 1$, we use the origin form (39) for the first integral in (38) and the asymptotic form (40) for the second; in this range the second term is negligible compared to the first (i.e., the ratio of the second to the first is proportional to $1/ka << 1$). Similarly, in the corresponding form of $g = C + B$, we drop term B of (19) which is also of order $1/ka$ relative to the specular beam. Thus for $P = D =$ (42), the scattering amplitude and corresponding differential scattering cross section reduce to

$$g_{\pm}(\hat{r},\hat{v}) = \pm \left(\frac{1}{3}\right)\sqrt{\frac{ka}{2\pi}}\, e^{-i\pi/4}\, \ell \csc\Gamma \left[\tan\Gamma(\cos\theta_0 - \cos\theta)\right]^{1/2},$$

(43)

$$\sigma(\theta,\varphi;\theta_0\pi) = \frac{8\pi a \ell^2}{9\lambda}\left[\frac{\cos\theta_0 - \cos\theta}{\sin 2\Gamma}\right] \equiv \sigma(S).$$

The forms of (43) hold on the specular beam defined in (42). On this beam, the angle θ satisfies the inequalities

$$\begin{aligned} &2\Gamma - \theta_0 \le \theta \le 2\Gamma + \theta_0 \quad \text{for} \quad 0 \le \theta_0 \le \Gamma, \\ &\theta_0 \le \theta \le 2\Gamma + \theta_0 \quad \text{for} \quad \Gamma \le \theta_0 \le \pi - 2\Gamma, \\ &\theta_0 \le \theta \le 2\pi - (2\Gamma + \theta_0) \quad \text{for} \quad \pi - 2\Gamma \le \theta_0 \le \pi - \Gamma, \end{aligned} \tag{44}$$

The lower limits of θ occur for $\varphi = \pi$; the upper limits occur for $\varphi = 0$ in the first two cases, and for $\varphi = \pi$ in the third. The total range of variation of θ is $2\theta_0$ in the first range, 2Γ in the second, and $2(\pi - \Gamma - \theta_0)$ in the third. Consequently the beam is nearly conical for small ranges of variation (in particular, for $\theta_0 = 0$ the beam is identically the cone of half angle 2Γ), and σ of (43) is slowly varying. The extreme values of $\sigma(S)$ are

$$\begin{aligned} \sigma(S)_{max} &= \frac{8\pi \ell^2 a}{9\lambda} \tan\Gamma \sin(\Gamma + \theta_0) \\ \sigma(S)_{min} &= 0, \qquad \theta_0 > \Gamma \\ &= \frac{8\pi \ell^2 a}{9\lambda} \tan\Gamma \sin(\Gamma - \theta_0), \qquad \theta_0 \le \Gamma . \end{aligned} \tag{45}$$

When $\frac{1}{2}\sigma(S)_{max} > \sigma(S)_{min}$ the value of θ corresponding to half power is defined by

$$\cos\theta = \cos\theta_0 - \sin(\Gamma + \theta_0)\sin\Gamma . \tag{46}$$

A crude, but simple, approximation for the differential scattering cross section for a constant value of φ, and D not too greatly different from P, is given by

$$\sigma = \sigma(S)\left|I[ka(P-D)]\right|^2, \quad \varphi = \text{constant}, \tag{47}$$

i.e., by the specular form $\sigma(S)$ "modulated" by the pattern factor $|I|^2$. In addition for some problems we can exploit the slow variation of θ on the beam and replace $\sigma(S)$ by $\sigma_{max}(S)$. More generally, we use

$$g(\hat{r},\hat{v}) = \left(\frac{2}{3}\right)\sqrt{\frac{ka}{2\pi D}}\, e^{i\pi/4}\, \ell\beta(\varphi_s) I[ka(P-D)], \quad \sigma(\theta,\varphi;\theta_s\pi) = \frac{4\pi a \ell^2}{9\lambda}\left(\frac{4\beta^2}{D}\right)\left|I[ka(P-D)]\right|^2 \tag{48}$$

In particular, in the plane containing the direction of incidence and the cone's axis, we have

$$g_{\pm}(\hat{r},\hat{v}) = \pm\frac{2\ell}{3} e^{-i\pi/4}\sqrt{\frac{ka}{2\pi(\sin\theta_0+\sin\theta)}}\, I[k\ell\cos(\theta_0+\Gamma)-k\ell\cos(\theta-\Gamma)]\begin{cases}\sin(\theta-\Gamma)\\ \sin(\theta_0+\Gamma)\end{cases}$$

$$\sigma_{\pm} = \frac{4\pi a\ell^2}{\lambda}\,\frac{(4/9)\left|I[k\ell\cos(\theta_0+\Gamma)-k\ell\cos(\theta-\Gamma)]\right|^2}{\sin\theta_0+\sin\theta}\begin{cases}\sin^2(\theta-\Gamma)\\ \sin^2(\theta_0+\Gamma)\end{cases} \tag{49}$$

Because of the variation of the angular factor β^2/D in σ of (48), the maximum of σ for fixed φ does not occur precisely in the specular direction (e.g., for one of the special cases of (49) we have $\beta^2/D = \sin^2(\theta-\Gamma)/(\sin\theta_0+\sin\theta)$, which does not have its maximum in the specular direction $\theta = \theta_0+2\Gamma$). However, for large values of ka this displacement will be obscured by the more or less "delta function like" behavior of $|I|^2$ around the specular value. Consequently, for most applications, the specular value may be taken as the maximum for a given φ.

In the above analysis, based on the condition $P \approx D$, we kept only the first I term of (38). Similarly, the second term of (38) would dominate were $P \approx -D$. However, the directions (θ,φ) for which $P = -D$ correspond to specular reflection from the internal surface, and (although of interest for reflection by a concave conical reflector) are not germane for our purposes.

Doubly truncated cone: The results for the finite cone can be extended immediately to treat doubly truncated cones specified by two radii a and a' such

that $a' = \delta a$, $\delta \leq 1$. Thus the amplitude corresponding to C of (16) is given by

$$C = \frac{-ik\delta \sin\Gamma}{2\pi}\left(\int_0^{a\csc\Gamma} - \int_0^{a'\csc\Gamma}\right) r' F(r';k)\,dr' ; \tag{50}$$

i.e., by the difference of two cone results. Consequently, we simply replace $I[x]$ in our previous results by

$$I[x,\delta] = \left\{ I[x] - \delta^{3/2} I[\delta x] \right\} \frac{1}{1-\delta} . \tag{51}$$

In particular, corresponding to σ of (48) we now have

$$\sigma_\delta(\theta,\pi;\theta_0,\pi) = \frac{4\pi a \ell^2}{9\lambda}\left(\frac{4\beta^2}{D}\right)\frac{1}{(1-\delta)^2}\left| I[ka(P-D)] - \delta^{3/2} I[\delta ka(P-D)] \right|^2 , \tag{52}$$

which reduces to

$$\sigma_\delta(s) = \frac{8\pi a \ell^2}{9\lambda}\left[\frac{\cos\theta_0 - \cos\theta}{\sin 2\Gamma}\right]\left(\frac{1-\delta^{3/2}}{1-\delta}\right)^2 \tag{53}$$

on the specular beam $P = D$.

For small δ the present cross section σ_δ differs from the previous by a term which is proportional to δ; for $\delta = 0$, σ_δ reduces to σ of (48). Near the other limit $\delta \approx 1$ (i.e., when $\Gamma \approx 0$ and the doubly truncated cone is approximately a circular cylinder), P is large and we use the asymptotic form (40) for the integrals in (52) to obtain the leading term

$$\sigma_\delta = \frac{\pi a \ell^2}{\lambda}\left(\frac{4\beta^2}{D}\right)\left| \frac{e^{ik\ell\sin\Gamma(P-D)/2} - \delta^{1/2} e^{-ik\ell\sin\Gamma(P-D)/2}}{2[k\ell\sin\Gamma(P-D)/2]} \right|^2 , \quad \delta \approx 1 \tag{54}$$

In the limit $\delta \to 1$, (54) reduces to the cross section for a finite cylinder:

$$\begin{Bmatrix} \sigma_\parallel(\theta,\varphi;\theta_0,\pi) \\ \sigma_\perp(\theta,\varphi;\theta_0,\pi) \end{Bmatrix} = \frac{4\pi a \ell^2}{\lambda D^3}\left(\frac{\sin Z}{Z}\right)^2 \begin{Bmatrix} A^2 \sin^2\theta \\ \sin^2\theta (A\cos\varphi + B\sin\varphi)^2 \end{Bmatrix} , \tag{55}$$

where ℓ is the length of the cylinder, and where

$$Z = \frac{k\ell}{2}(\cos\theta_0 - \cos\theta) . \tag{56}$$

In the specular direction (i.e., on the cone $\theta = \theta_0$) (55) reduces to

$$\sigma_\parallel(\theta_0,\varphi;\theta_0,\pi) = \frac{(4\pi)a\ell^2}{2\lambda}\sin\theta_0 \cos\frac{\varphi}{2} . \tag{57}$$

2.3. Elementary Considerations

It is of interest to compare the cylinder result (57) for $\varphi = 0$ with the corresponding result for the singly-truncated cone

$$\sigma_1(\theta_0,0;\theta_0,\pi) = (4\pi)\frac{a\ell^2}{2\lambda}\sin\theta_0$$

(58)

$$\sigma(2\Gamma+\theta_0,0;\theta_0,\pi) = 4\pi\left(\frac{2\ell^2 a}{9\lambda}\right)\frac{\sin(\theta_0+\Gamma)}{\cos\Gamma} .$$

We first rotate the cone through the angle Γ as in Figure 4, to obtain a geometry in which $\theta_0+\Gamma$ for the cone corresponds to θ_0 for the cylinder, i.e., for either case we are concerned with the sine of the angle with the reflecting generator. Thus the two expressions differ in that the cylinder result contains $a/2$ while that for the cone contains $(2/9)a\sec\Gamma$. The cone contains $a\sec\Gamma$ because the radius of curvature in the plane containing the surface normal at some slant height ℓ' is not a' but $a'\sec\Gamma$. In order to interpret the additional factor $4/9$ (as well as the more complicated factor $4(1-\delta^{3/2})^2/(1-\delta)^2 9$ which occurs in (53) for the doubly truncated cone) it is convenient to give an elementary derivation of σ for the cone based more or less on the result σ_1 for the cylinder. Thus if we start essentially with the "geometrical optics scattering amplitude" for reflection from a point on a cylindrical surface, i.e., with a function proportional to $\sqrt{\rho}$ (where ρ is the radius of the curvature at the point), and integrate ρ between 0 and a, we obtain $2\sqrt{a/3}$. The corresponding value of σ is thus proportional to $4a/9$. We do this explicitly in the following.

According to geometrical optics, the reflection of a ray from a point on a perfectly reflecting surface, at which one radius of curvature is infinite, is specified in general by[10]

$$\sigma = 4\pi\rho\cos\alpha\left[\rho\left(\frac{1}{R_t}+\frac{1}{R_r}\right)^2\cos\alpha + 2\left(\frac{1}{R_t}+\frac{1}{R_r}\right)\sin^2\gamma\right]^{-1}, \tag{59}$$

where ρ is the finite radius of curvature at the point of reflection, γ is the angle with the surface tangent in the plane in which the radius of curvature is infinite, α is the angle of incidence with the normal, and R_t and R_r are the distances introduced previously. If the distances are large compared to ρ, then (59) reduces to

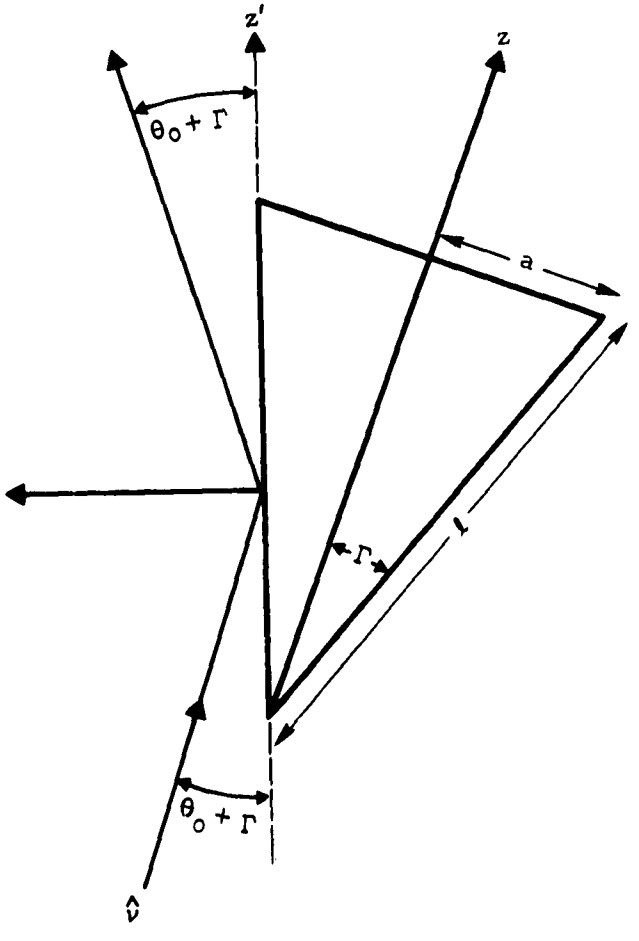

Figure 4. Scattering at the specular angle.

(60) $$\sigma = 2\pi\rho\cos\alpha \Big/ \left(\frac{1}{R_t} + \frac{1}{R_r}\right)\sin^2\gamma, \quad \rho \ll R_t, R_r .$$

This expression differs from σ_1 of (57) by the factor

(61) $$C = \frac{\ell^2}{\lambda}\sin^2\gamma\left(\frac{1}{R_t} + \frac{1}{R_r}\right) .$$

This "conversion factor" takes into account that (60) corresponds to a "near-field" cylindrical wave whereas (57) corresponds to a three-dimensional wave form; see reference 10 for detailed discussion.

In order to take into account the fact that a detector may receive rays from an extended portion of a surface having a variable radius of curvature, we replace (59) by the square of the function obtained by integrating the scattering amplitude over the appropriate range of ρ. (The amplitude g corresponding to (59) is obtained by evaluating the "near-field" form (10) by the method of stationary phase.) If the impact point is at a distance ξ from the tip of the cone, then the corresponding value of ρ is given by

(62) $$\rho(\xi) = \left(\frac{a}{\ell}\sec\Gamma\right)\xi .$$

For the case of a distant source and a distant receiver, each point of the generator corresponds to a stationary point of the original surface integral, and we must "sum" the individual field contributions. Thus the resultant amplitude may be written as

(63) $$g = \frac{1}{\ell}\int_0^{\ell} f(\xi)\,d\xi ,$$

where $f(\xi)$ is proportional to the square root of (60) times a phase factor. Since the phase factor and the angles γ and α are constant along the generator, and since

(64) $$\frac{d\xi}{\ell} = \frac{d\rho}{a\sec\Gamma} ,$$

the integral in (62) is simply

(65) $$\frac{1}{a\sec\Gamma}\int_0^{a\sec\Gamma}\sqrt{\rho}\;d\rho = \frac{2}{3}\sqrt{a\sec\Gamma} .$$

The corresponding scattering cross section is

(66) $$\sigma = \left(\frac{4}{9\cos\Gamma}\right)\left[2\pi a\cos\alpha \Big/ \left(\frac{1}{R_t}+\frac{1}{R_r}\right)\sin^2\gamma\right] ,$$

which differs from (60) only by the presence of the factor $4/(9\cos\Gamma)$, and from $\sigma(S)$ of (43) only by the conversion factor (61).

Similarly, for the doubly truncated cone, such that the radii of curvature of the extremities of the reflecting generator are equal to $a\sec\Gamma$ and $a'\sec\Gamma$, with $a' = \delta a$, the above procedure yields

(67) $$\sigma = \left(\frac{4}{9\cos\Gamma}\right)\left[2\pi a\cos\alpha \Big/ \left(\frac{1}{R_t}+\frac{1}{R_r}\right)\sin^2\gamma\right]\left(\frac{1-\delta^{3/2}}{1-\delta}\right)^2 ,$$

which includes the tipped cone result (66) $(\delta = 0)$ and the circular cylinder result (60) $(\delta = 1)$.

3. ELECTROMAGNETIC FIELDS

The electromagnetic case may be treated by applying the procedures of Section 2.1 to the vector analog of (5)[11]:

(68) $$\underset{\sim}{E}_s\cdot\underset{\sim}{e} = -\oint_S\left[\underset{\sim}{E}\times(\nabla\times\underset{\approx}{\Gamma}\cdot\underset{\sim}{e}) - \underset{\approx}{\Gamma}\cdot\underset{\sim}{e}\times(\nabla\times\underset{\sim}{E})\right]\cdot\hat{n}\,dS ,$$

where $\underset{\sim}{E}$ is the total electric field, and $\underset{\sim}{E}_s$ is the scattered field, and $\underset{\sim}{e}$ is an arbitrary vector. The function $\underset{\approx}{\Gamma}(\underset{\sim}{r},\underset{\sim}{r}') = \left[\underset{\approx}{I} - (\nabla\nabla'/k^2)\right]\mathcal{G}(|\underset{\sim}{r}-\underset{\sim}{r}'|)$ is the free space dyadic Green's function; $\underset{\approx}{I}$ is the unit dyadic, and $\mathcal{G}(|\underset{\sim}{r}-\underset{\sim}{r}'|)$ is given after (5). For a dipole source at $\underset{\sim}{r}_t$ oriented in the direction $\hat{b}$, say with $\hat{b}\cdot\hat{r}_t = 0$, we use

(69) $$\underset{\sim}{E}_o(\underset{\sim}{r},\underset{\sim}{r}_t) = \left(\underset{\approx}{I} - \frac{\nabla\nabla_t}{k^2}\right)\cdot\hat{b}\,\frac{e^{ik|\underset{\sim}{r}-\underset{\sim}{r}_t|}}{4\pi|\underset{\sim}{r}-\underset{\sim}{r}_t|} \sim \hat{b}\,\frac{e^{ikr_t}}{4\pi r_t}\,e^{ik\underset{\sim}{r}\cdot\hat{\nu}}, \quad \hat{\nu} = -\hat{r}_t ,$$

where the asymptotic form holds at large distances from the source. Then the vector scattering amplitude corresponding to (68) is defined by

(70) $$\underset{\sim}{E} \sim \left[\frac{e^{ikr_t}}{4\pi r_t}\right]\left[\frac{e^{ikr}}{r}\right]\underset{\sim}{g}(\hat{r},\hat{\nu}), \quad r_t\to\infty, \quad r\to\infty ;$$

in terms of $\underset{\sim}{g}$ the differential and total scattering cross sections are given by

(71) $$\sigma(\hat{r},\hat{\nu}) = 4\pi|\underset{\sim}{g}(\hat{r},\hat{\nu})|^2, \qquad Q(\nu) = \frac{4\pi}{k}\,\mathrm{Im}\,\hat{b}\cdot\underset{\sim}{g}(\hat{\nu},\hat{\nu}) .$$

Paralleling the previous section we approximate the surface fields in (68) by their geometrical values. For a perfect conductor we use the boundary condition $\hat{n}\times\underset{\sim}{E} = 0$, and the geometrical values

(72) $(\nabla\times\underset{\sim}{E})\times\hat{n} = 2(\nabla\times\underset{\sim}{E}_o)\times\hat{n}$ *on lit side,* $= 0$ *on dark side;*

thus we obtain the approximation

(73) $$\underset{\sim}{E}_s\cdot\underset{\sim}{e} = 2\int\underset{\sim}{\Gamma}\cdot e\times(\nabla\times\underset{\sim}{E}_o)\cdot\hat{n}dS.$$

The scattering amplitude associated with (73) is

(74) $$\underset{\sim}{g}_e = (\underset{\sim}{I}-\hat{r}\hat{r})\cdot(\hat{b}\times\hat{v})\times\underset{\sim}{f} = \underset{\sim}{f}\times(\hat{v}\times\hat{b})+\hat{r}\hat{r}\cdot(\hat{v}\times\hat{b})\times\underset{\sim}{f}\ ,$$

where

(75) $$\underset{\sim}{f} = \frac{ik}{2\pi}\int\hat{n}e^{ikr\cdot(\hat{v}-\hat{r})}dS.$$

The analogous results for the magnetic field follow from (73) by using Maxwell's equations; thus, for example, we obtain the scattering amplitude

(76) $$\underset{\sim}{g}_m = \hat{r}\times(\underset{\sim}{f}\times\hat{m}) = \hat{r}\cdot\hat{m}\underset{\sim}{f} - \hat{r}\cdot\underset{\sim}{f}\hat{m}\ ,$$

where $\hat{m}$ is the direction of the incident magnetic field.

In view of the similarity of (75) and (11) approximations for $\underset{\sim}{f}$ follow from our scalar results on replacing $\beta(\varphi_s)$ by $-\hat{n}(\varphi_s)$. Thus corresponding to (48) we obtain $\underset{\sim}{f} = -[g(48)/\beta(\varphi_s)]\hat{n}(\varphi_s)$ which leads to

(77) $$\underset{\sim}{g}_m = \left\{\hat{r}\times[\hat{m}\times\hat{n}(\varphi_s)]\right\}\frac{g(48)}{\beta(\varphi_s)}\ ,\qquad \underset{\sim}{g}_e = \left\{(\hat{v}\times\hat{b})\times\hat{n}(\varphi_s) - \hat{r}\hat{r}\cdot(\hat{v}\times\hat{b})\times\hat{n}(\varphi_s)\right\}\frac{g(48)}{\beta(\varphi_s)}.$$

For observation in the plane defined by the direction of incidence and the cone's axis, we replace $g(48)$ in (77) by $g(49)$. If, in addition, $\hat{m} = \hat{y}$ we obtain the amplitudes and cross sections given in (78):

(78) $$\underset{\sim}{g}_m = g_+(49)\hat{y},\quad \sigma_m = \sigma_+(49),\quad \underset{\sim}{g}_e = -g_+(49)(\sin\tau\hat{t}-\cos\tau\hat{n}),\quad \sigma_e = \sigma_+(49),$$

where $\hat{t}$ is the direction of the reflecting generator, and $\hat{r}\cdot\hat{t} = \cos\tau$. Similarly if $\hat{b} = \hat{y}$

(79) $$\underset{\sim}{g}_m = g_-(49)(\sin\tau\hat{t}-\cos\tau\hat{n}),\quad \sigma_m = \sigma_-(49),\quad \underset{\sim}{g}_e = g_-(49)\hat{y},\quad \sigma_e = \sigma_-(49).$$

4. NUMERICAL ILLUSTRATIONS

In this section we illustrate the use of our results by applying them to the cone with parameters $\Gamma = 10.5^\circ$ and $\ell = 89.18''$, for $k\ell = 142.2$ (i.e., S-band, $\lambda = 3.937''$). Initially we consider $\sigma(S)$ of (43), the scattering cross section on the specular beam; then we consider the more general case.

In order to apply (43) we first determine the specular beam by using (42). Specializing (42) to the present value $\Gamma = 10.5^\circ$ for different values of θ_o, leads to the results shown in Figures 5 and 6; here we have plotted the intersections of the beams with planes perpendicular to the cone's axis. From these graphs we can determine θ, and consequently obtain $\cos\theta_o - \cos\theta$ which specifies the angular behavior of $\sigma(S)$. Figures 7 and 8 show the variation of $\cos\theta_o - \cos\theta$ on the beams of Figures 5 and 6.

In the above example the cross section is seen to be slowly varying on the specular beam. A measure of the variation of $\sigma(S)$ (i.e., of the intensity around the "rim" of the "specular funnel") is given by the angular separation of the half power directions as a function of θ_o and Γ. Solving (42) and (46) simultaneously yields the results of Figures 9 and 10 which show that $\sigma(S)$ is slowly varying over relatively large ranges of Γ and θ_o. (These graphical results can of course be used for specific applications; e.g., from Figures 9 and 10 the half power directions for $(\Gamma, \theta_o) = (25^\circ, 70^\circ)$ are found to be $(\theta, \varphi) = (94^\circ, \pm 125^\circ)$.)*

As another illustration we consider observation off the specular beam in the plane defined by the direction of incidence and the cone's axis. In particular, for $\theta_o = 0$ (nose-on incidence) Figure 11 shows $\sigma_\pm$ of (49), and $\sigma(S)|I|^2$ of (47). Similarly, for $\theta_o = 0$, Figure 12 compares an auxilliary function $\sigma_\ell \equiv \pi|q_+ - q_-|^2$ with $\sigma(S)|I|^2$, and Figure 13 gives the corresponding

*In practice, photo-optical techniques facilitate determining $\theta(S)$ and $\sigma(S)$. Thus one can illuminate a silvered cone with a distant point source of light and record the specular beams on photographic paper or film. If the paper is oriented perpendicular to the cone's axis, then the recorded traces give directly the variation of $\theta(S)$ (essentially as in Figures 5 and 6). Using positive transparencies and controlled processing yields traces which can be measured on an optical densitometer for direct determinations of $\sigma(S)$.

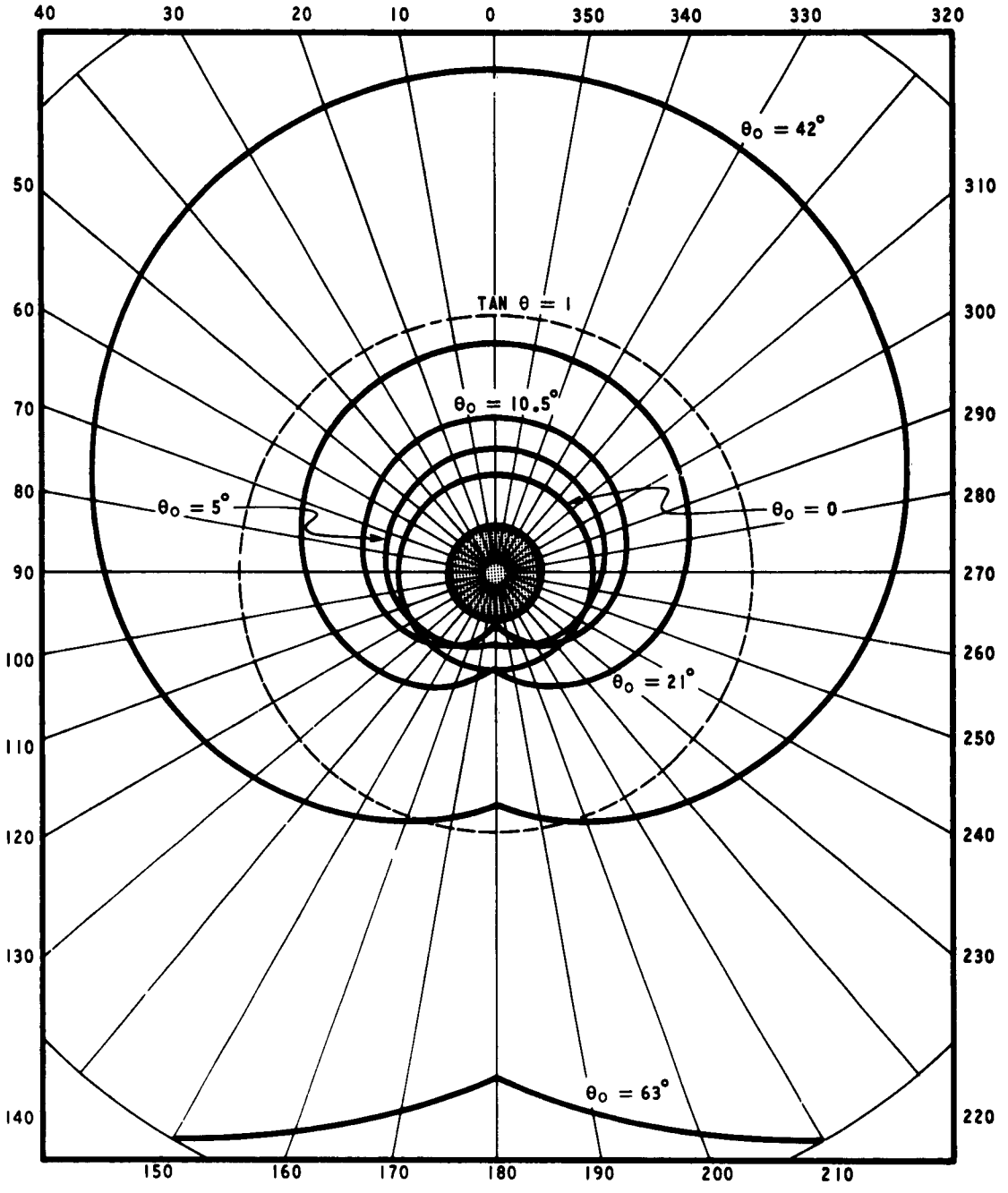

Figure 5. Traces of some specular beams on the plane $z = 1$ for $\Gamma = 10.5^{\circ}$ and $\theta_o < \pi/2$; the angular and radial coordinates are respectively φ and $\tan\theta$. The shaded region corresponds to the cross section of the scatterer.

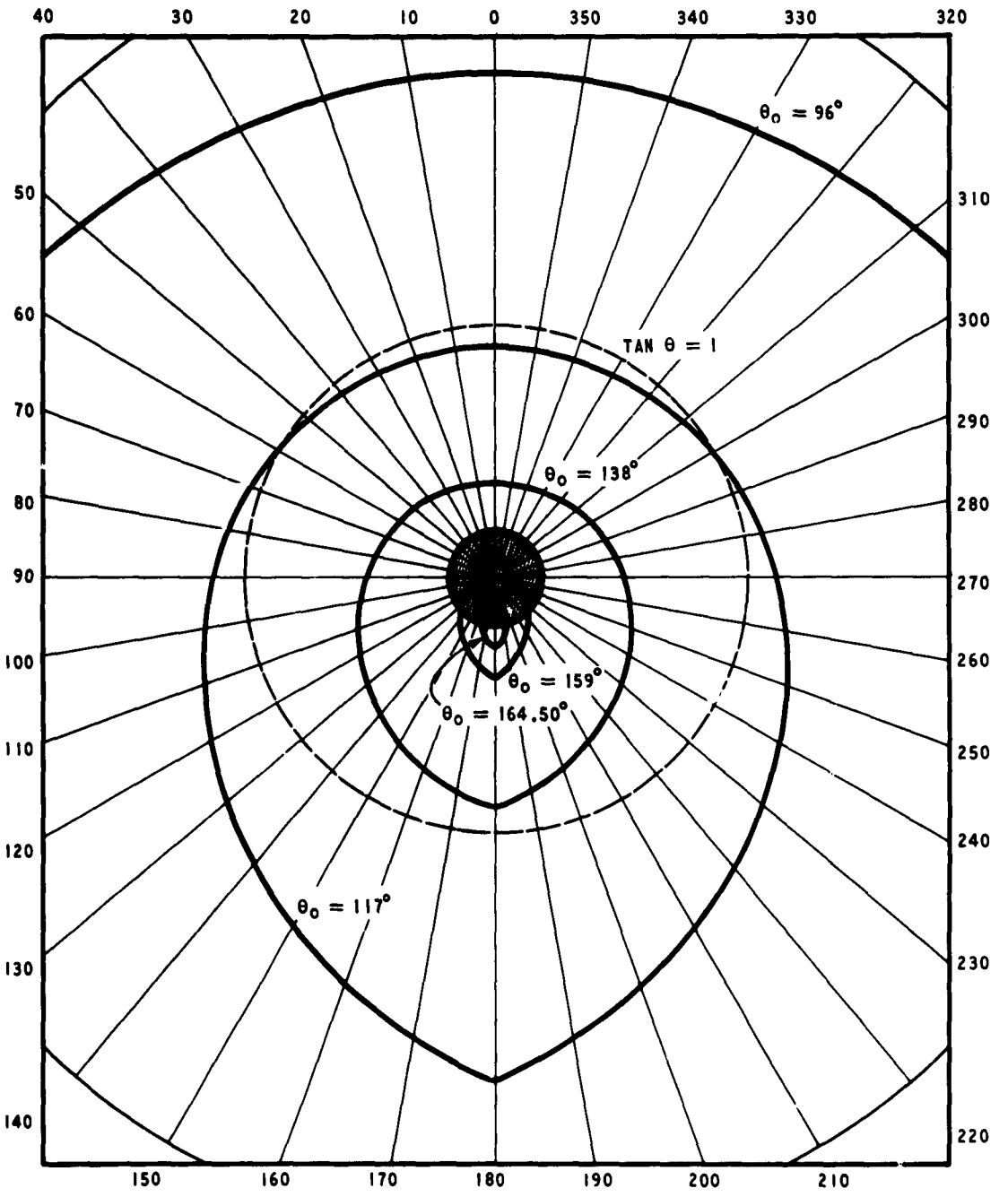

Figure 6. Traces of some specular beams on the plane $z = -1$ for $\Gamma = 10.5^{\circ}$ and $\theta_0 > \pi/2$; the angular and radial coordinates are respectively φ and $\tan\theta$. The shaded region corresponds to the cross section of the scatterer.

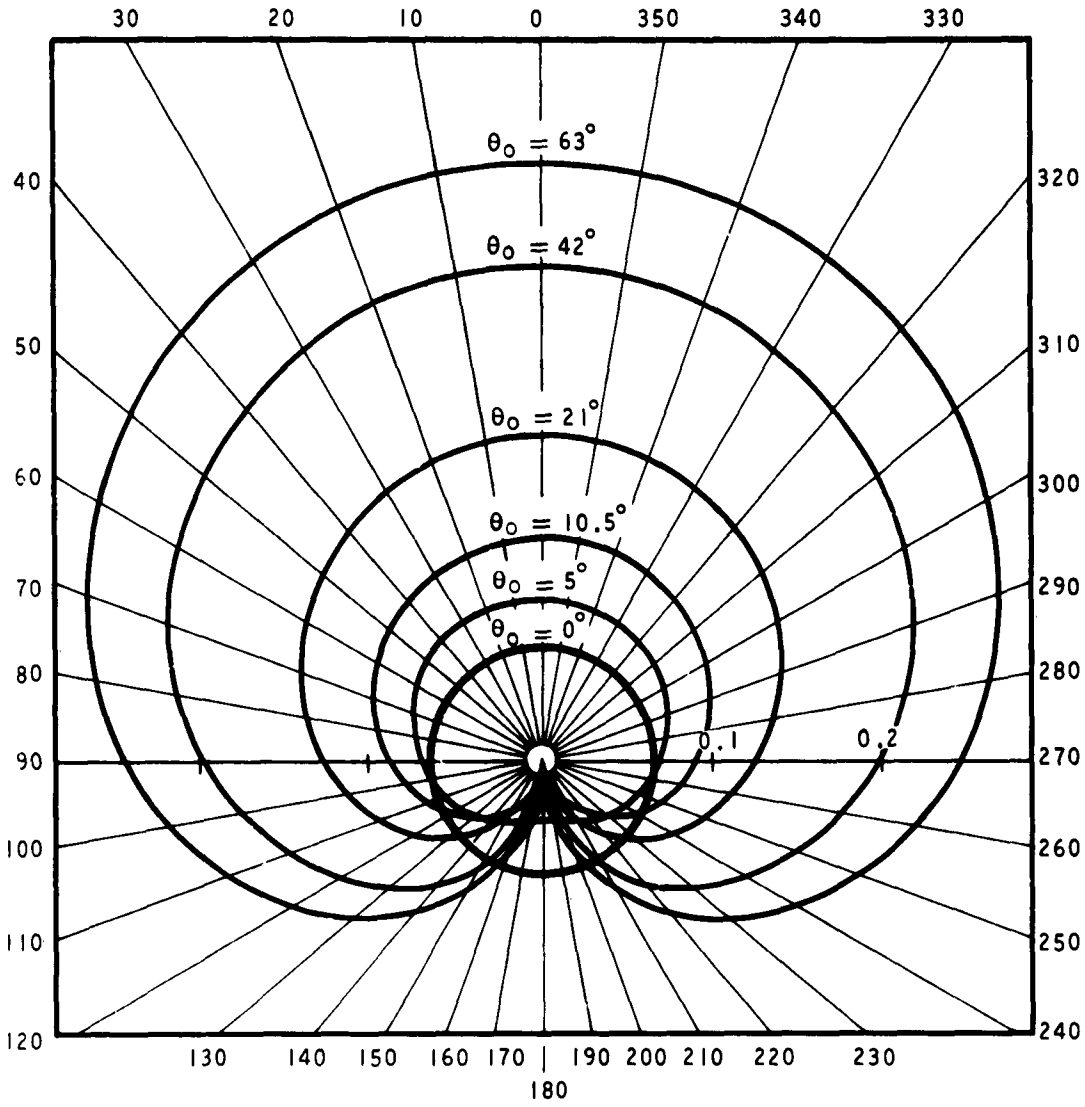

Figure 7. The variation of $\cos\theta_o - \cos\theta$ on the beams of Figure 5; the angular and radial coordinates are respectively φ and $\cos\theta_o - \cos\theta$.

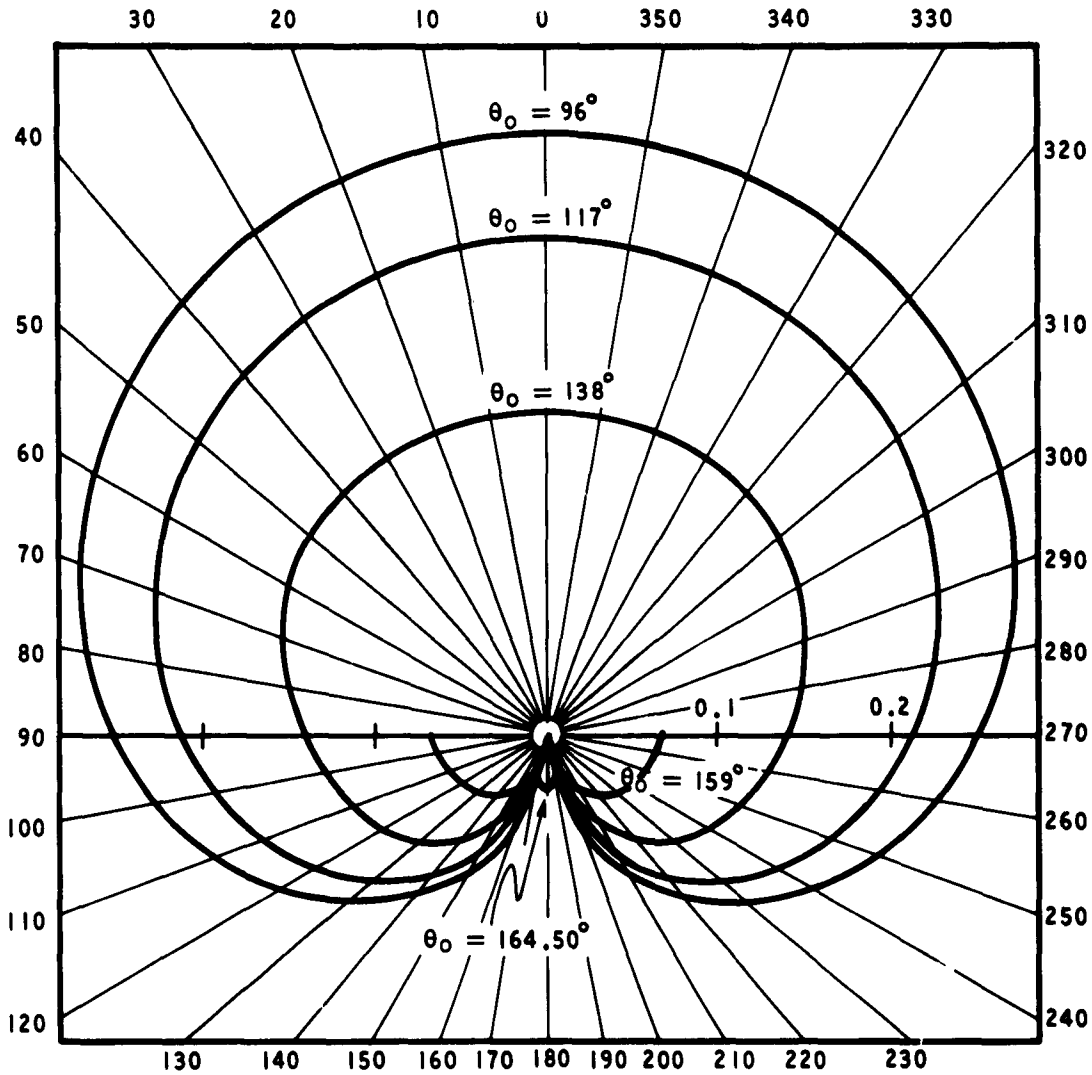

Figure 8. The variation of $\cos\theta_0 - \cos\theta$ on the beams of Figure 6; the angular and radial coordinates are respectively φ and $\cos\theta_0 - \cos\theta$.

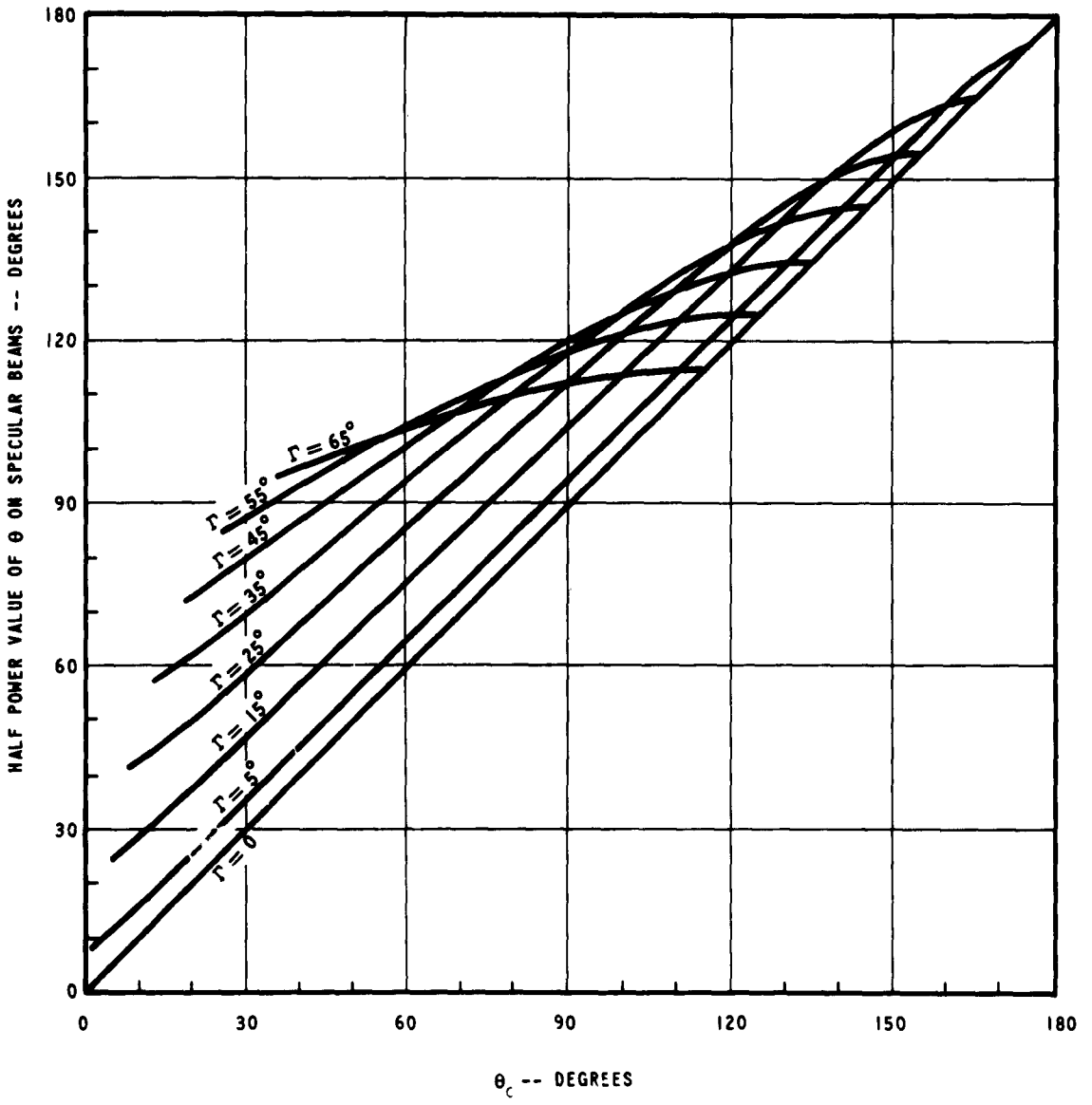

Figure 9. Half power values of θ on specular beams as a function of Γ and θ_o.

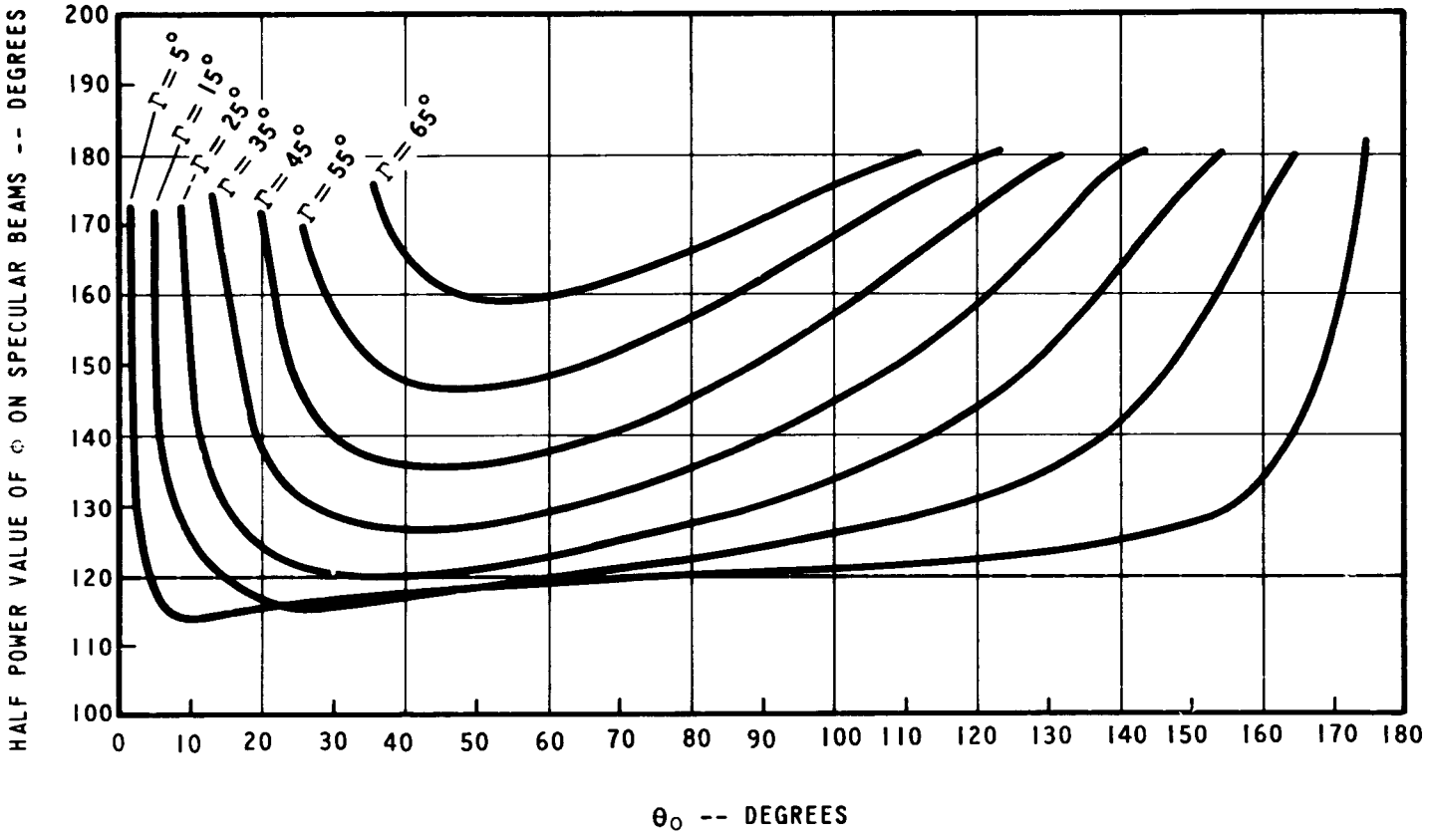

Figure 10. Half power values of Φ on specular beams as a a function of Γ and θ_o.

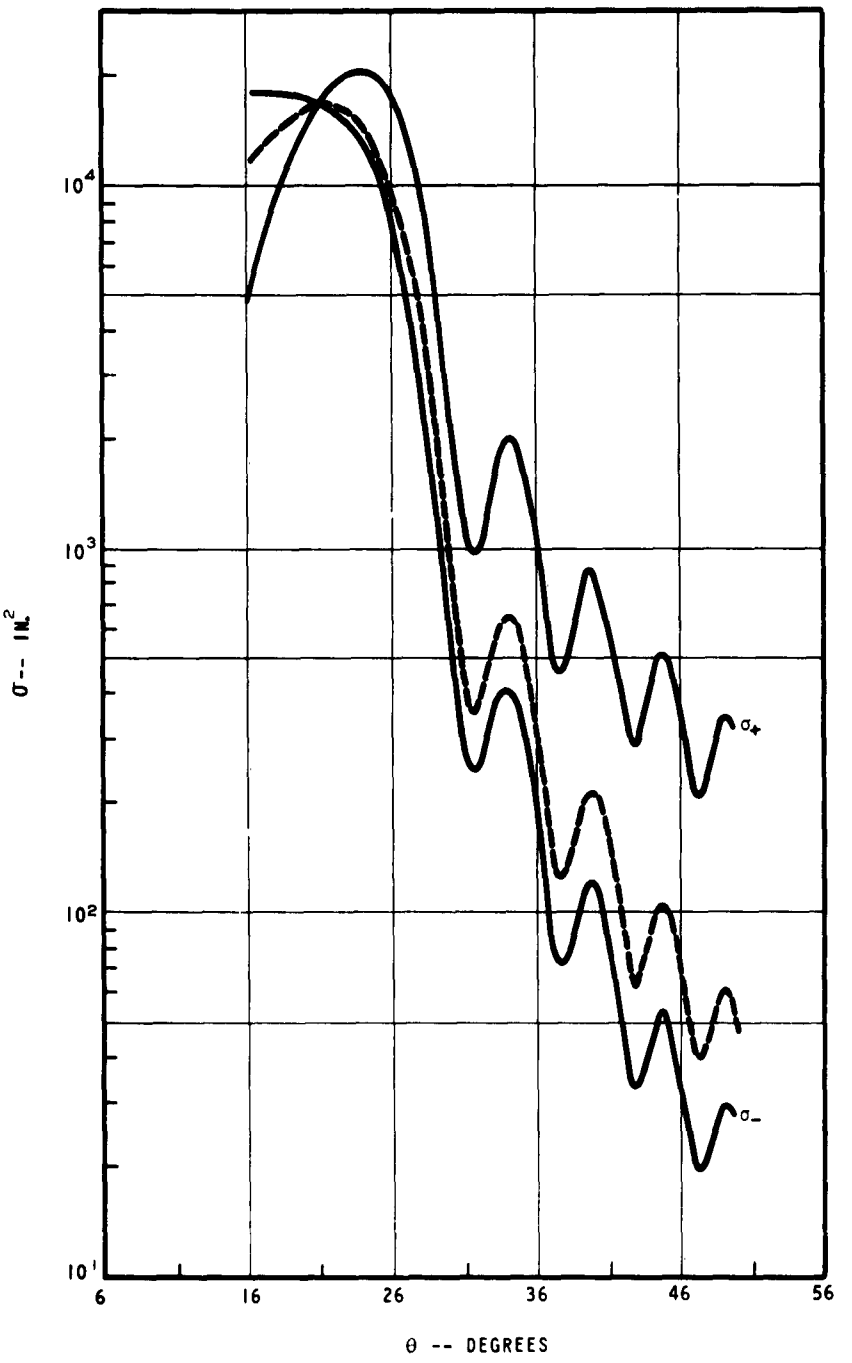

Figure 11. $\sigma_{\pm}$, and $\sigma\ (s)|I|^2$, for $\theta_o = 0$ and $\varphi = 0$; here and on the following graphs, the dashed curve represents $\sigma\ (s)|I|^2$.

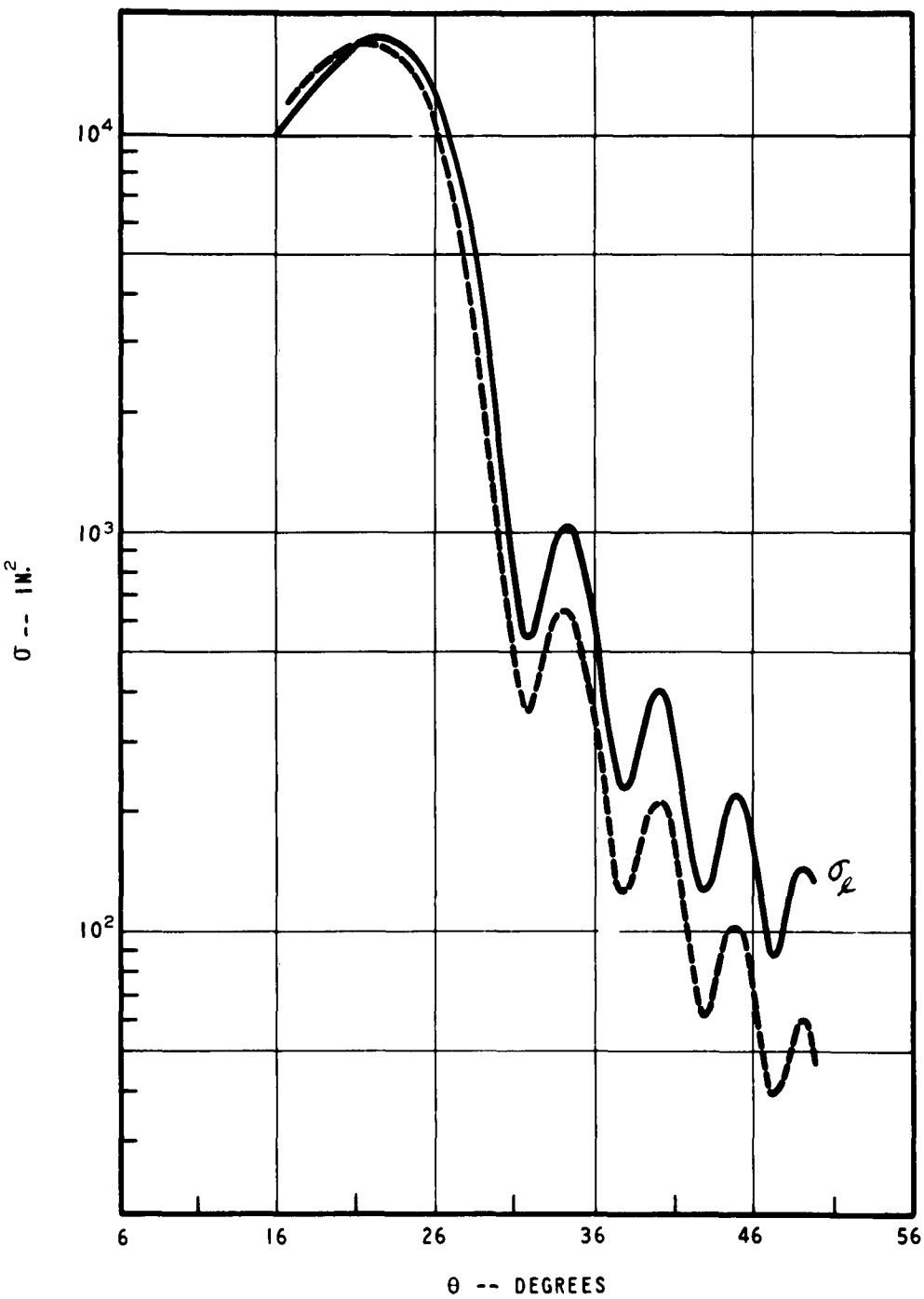

Figure 12. σ_ℓ and $\sigma(s)|I|^2$, for $\theta_o = 0$ and $\varphi = 0$.

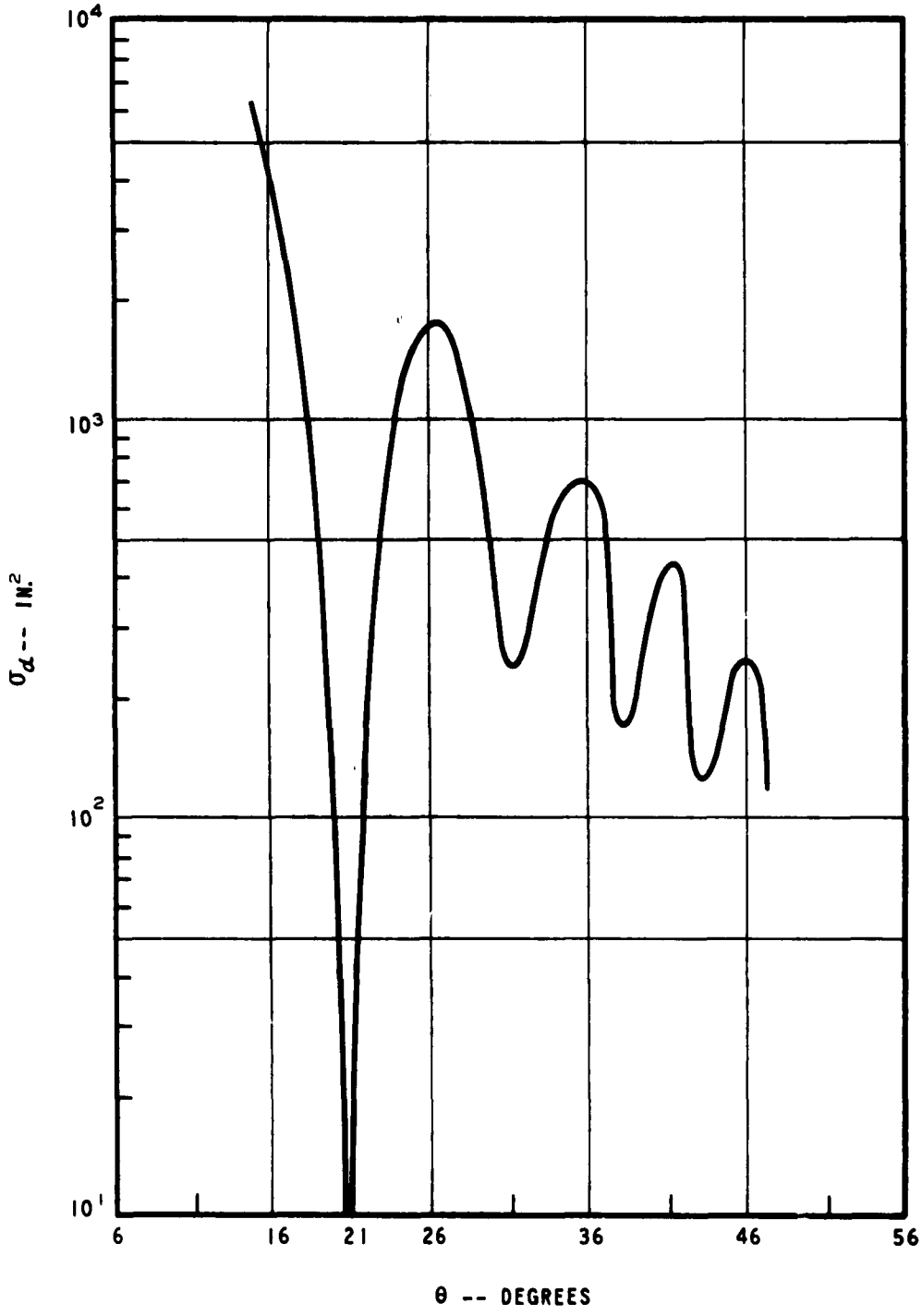

Figure 13. σ_d for $\theta_o = 0$ and $\varphi = 0$.

function $\sigma_a \equiv \pi|g_+ + g_-|^2$. These auxilliary functions are constructed from g_+ and g_- of (49), or equivalently, by using either β_L or β_D in (48); the functions σ_ℓ and σ_a differ from the "reflected component" and "shadow forming component" introduced previously in that they are based on the approximate forms (48) and (49) instead of (11'). The analogous sets of curves for $\theta_0 = 42^\circ$, and $\pi - 42^\circ$ are given in Figures 14 to 16, and 17 to 19, respectively.

The results for $\theta_0 = 0$ illustrate a situation where the shadow forming field has some effect near the specular direction; i.e., the present cone ($\Gamma = 10.5^\circ$) is relatively narrow, and consequently the specular direction ($\theta = 21^\circ$) occurs relatively near the forward direction where σ_a is a maximum. Thus the curves σ_+ and σ_- of Figure 11 which correspond to the interference pattern of σ_ℓ of Figure 12 and σ_a of Figure 13 are relatively different and their maxima are shifted from that of σ_ℓ. The maximum of σ_ℓ does not occur at the specular value (as does that of $\sigma(S)|I|^2$) because of the variation of the angular factor β_L (which is neglected in $\sigma(S)|I|^2$).

On the other hand for the non-axial cases, Figures 14, 15, 17, and 18 show that the shadow forming component is negligible in the vicinity of the specular direction (and is significant only near the forward direction). The maxima of $\sigma(S)|I|^2$, σ_+, σ_-, and σ_ℓ practically coincide at the specular angle, and the curves differ negligibly over broad ranges of θ. Thus we may use the simplest function $\sigma(S)|I|^2$ as a good approximation for any of the other three (an approximation that is even better for larger Γ and/or $k\ell$ than used for the figures). Consequently the oscillatory function $|I|^2$ is the dominant factor of the scattering patterns. Thus, for many practical applications, $|I|^2$ may be regarded as a "universal function" for the cone in the sense that $|(\sin x/x)|^2$ and $|2J_1(x)/x|^2$ are used for the strip and disk.

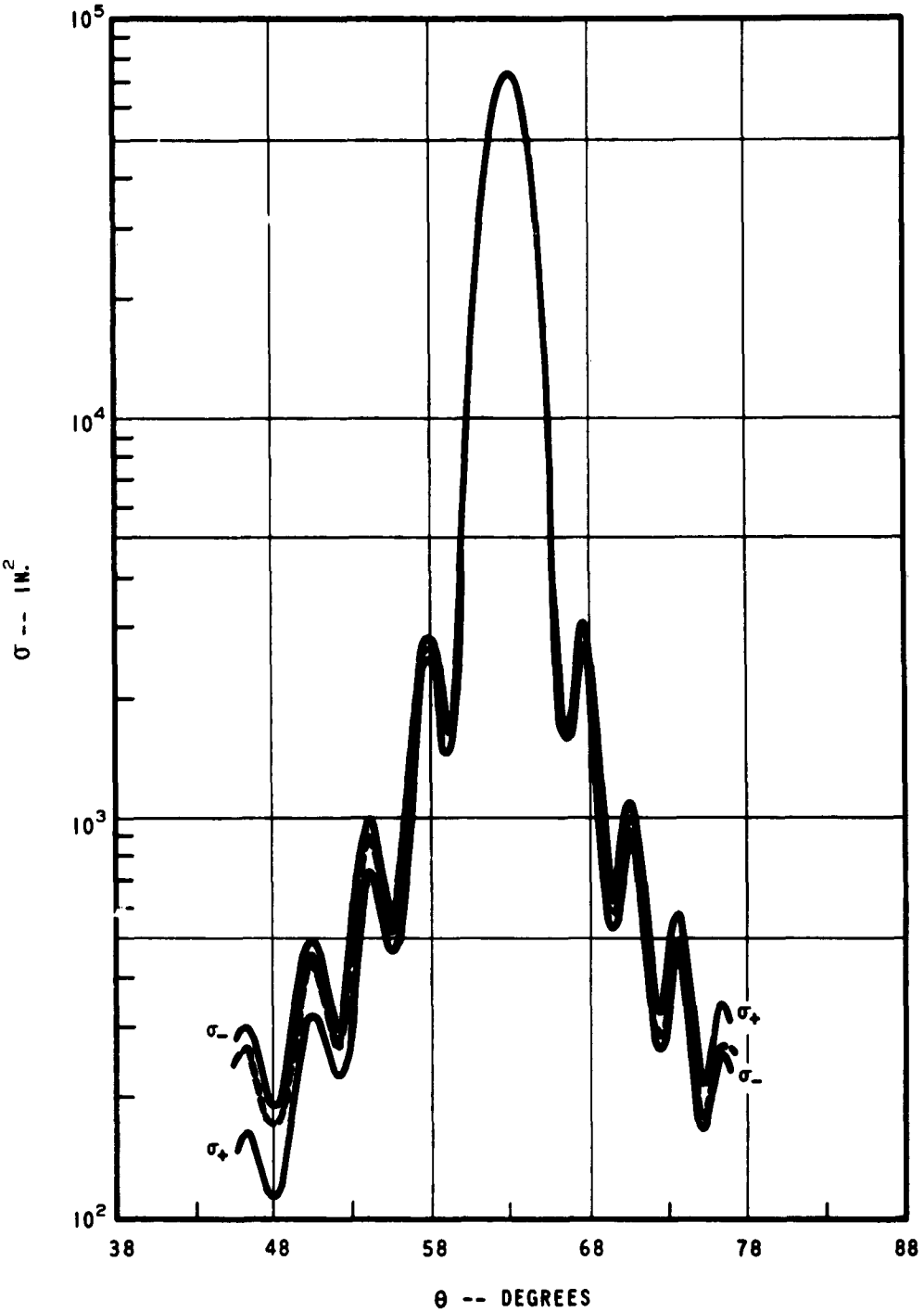

Figure 14. $\sigma_\pm$ and σ (s)$|I|^2$, for $\theta_o = 42^\circ$ and $\varphi = 0$.

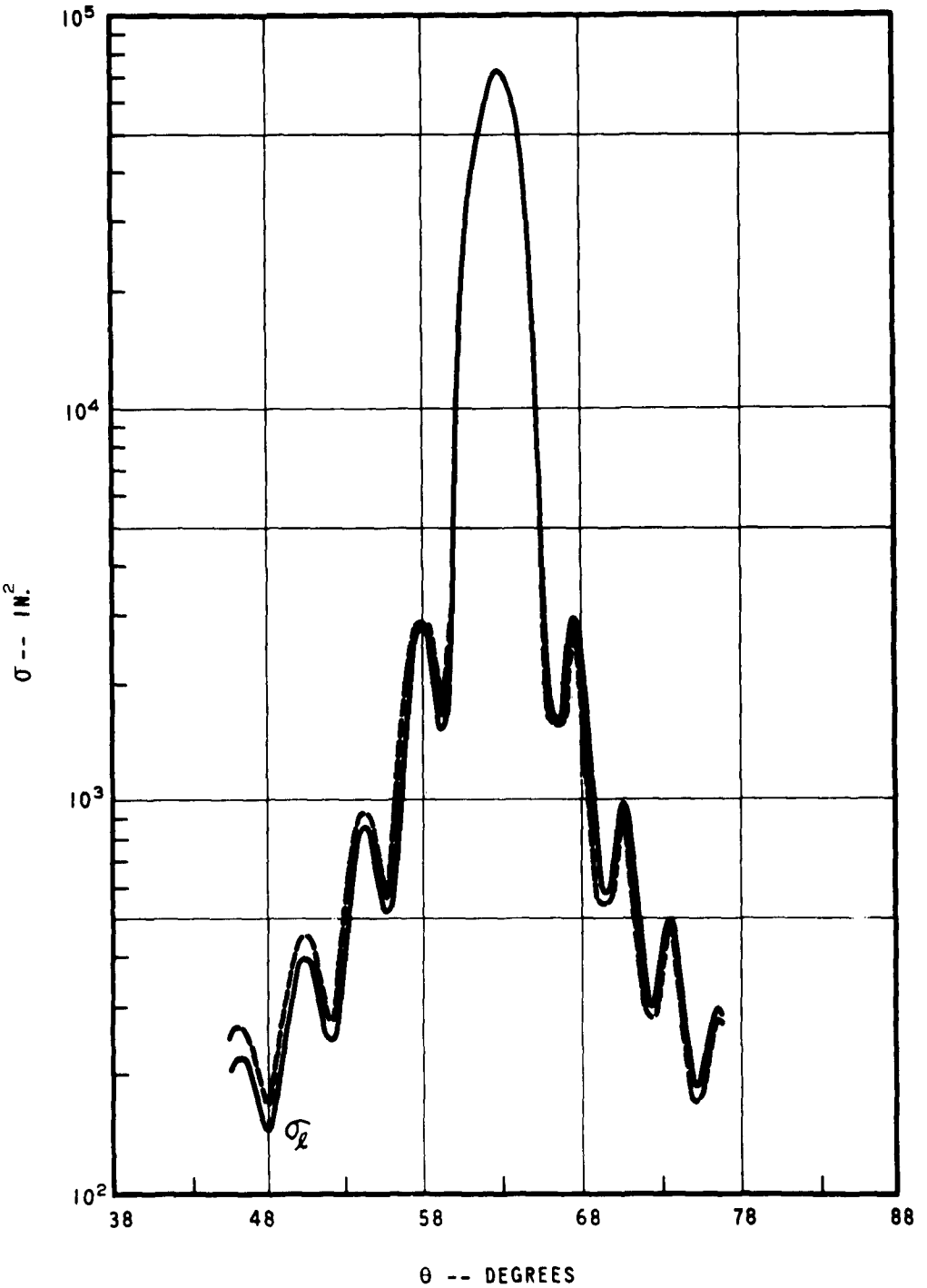

Figure 15. σ_ℓ and $\sigma(s)|I|^2$, for $\theta_o = 42^\circ$ and $\varphi = 0$.

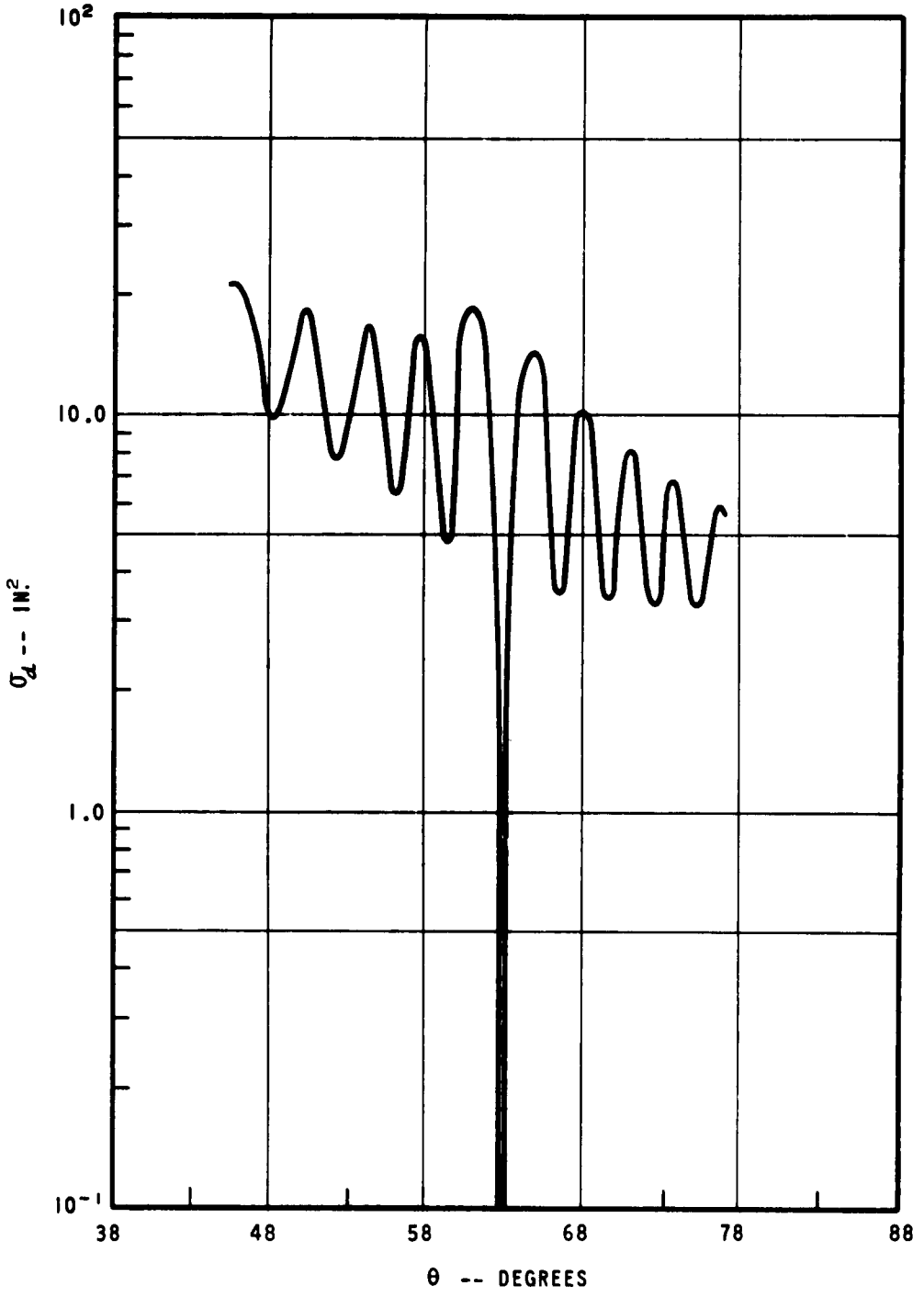

Figure 16. σ_d for $\theta_o = 42^\circ$ and $\varphi = 0$.

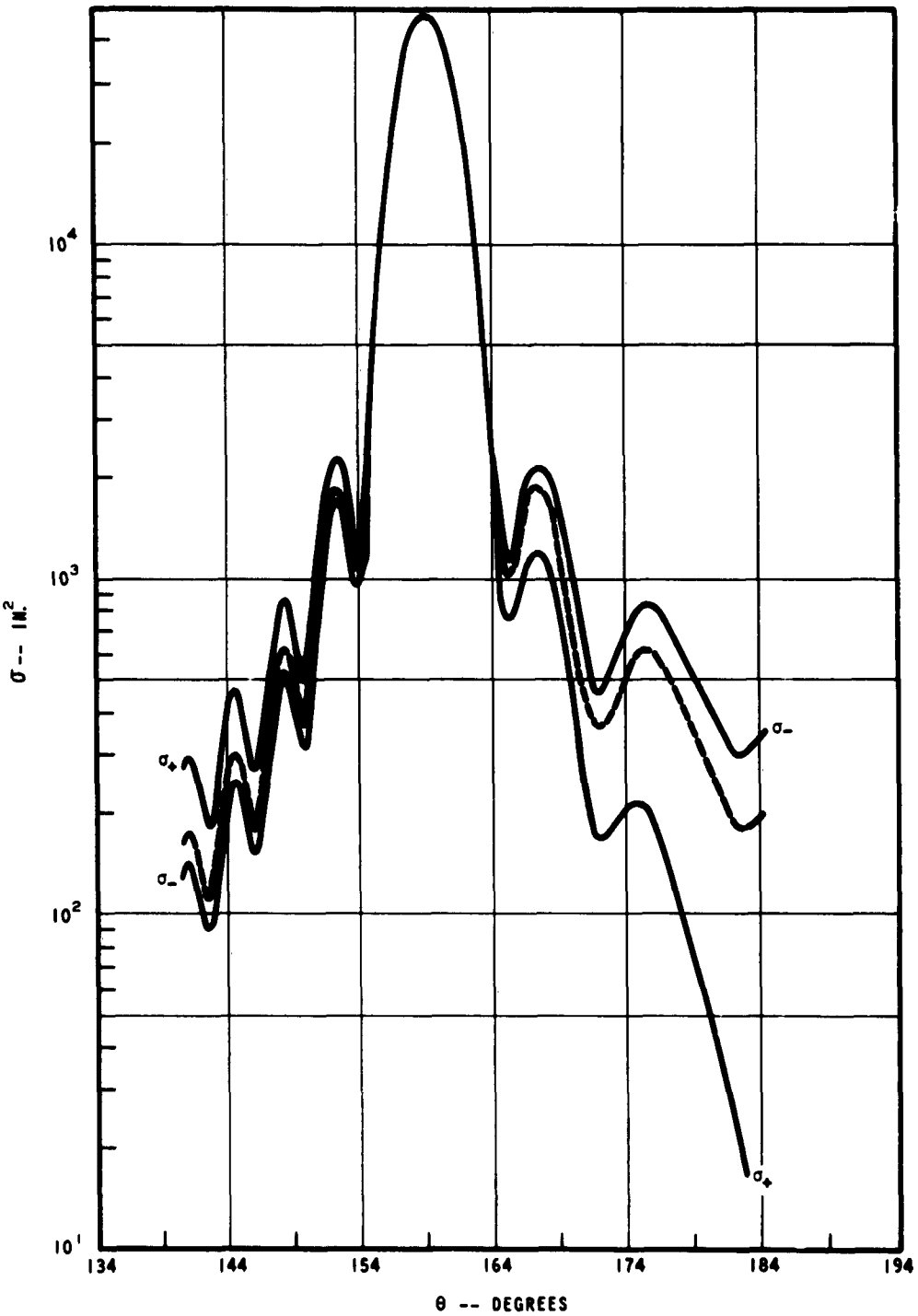

Figure 17. $\sigma_{\pm}$ and $\sigma(s)|I|^2$ for $\theta_o = \pi - 42^o$, and $\varphi = 0, \pi$.

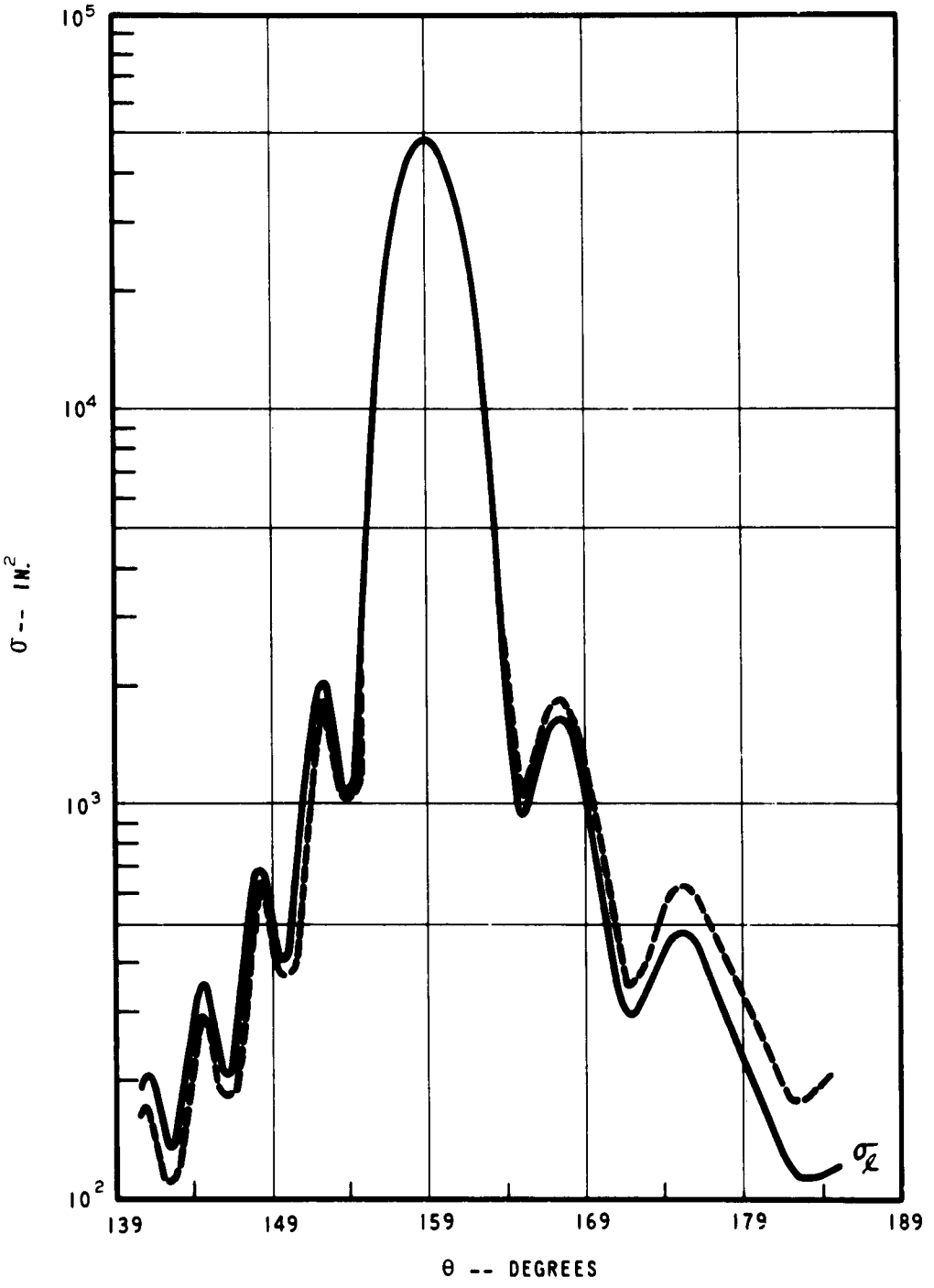

Figure 18. σ_ℓ and $\sigma(s)|I|^2$ for $\theta_o = \pi - 42^\circ$, and $\varphi = 0, \pi$.

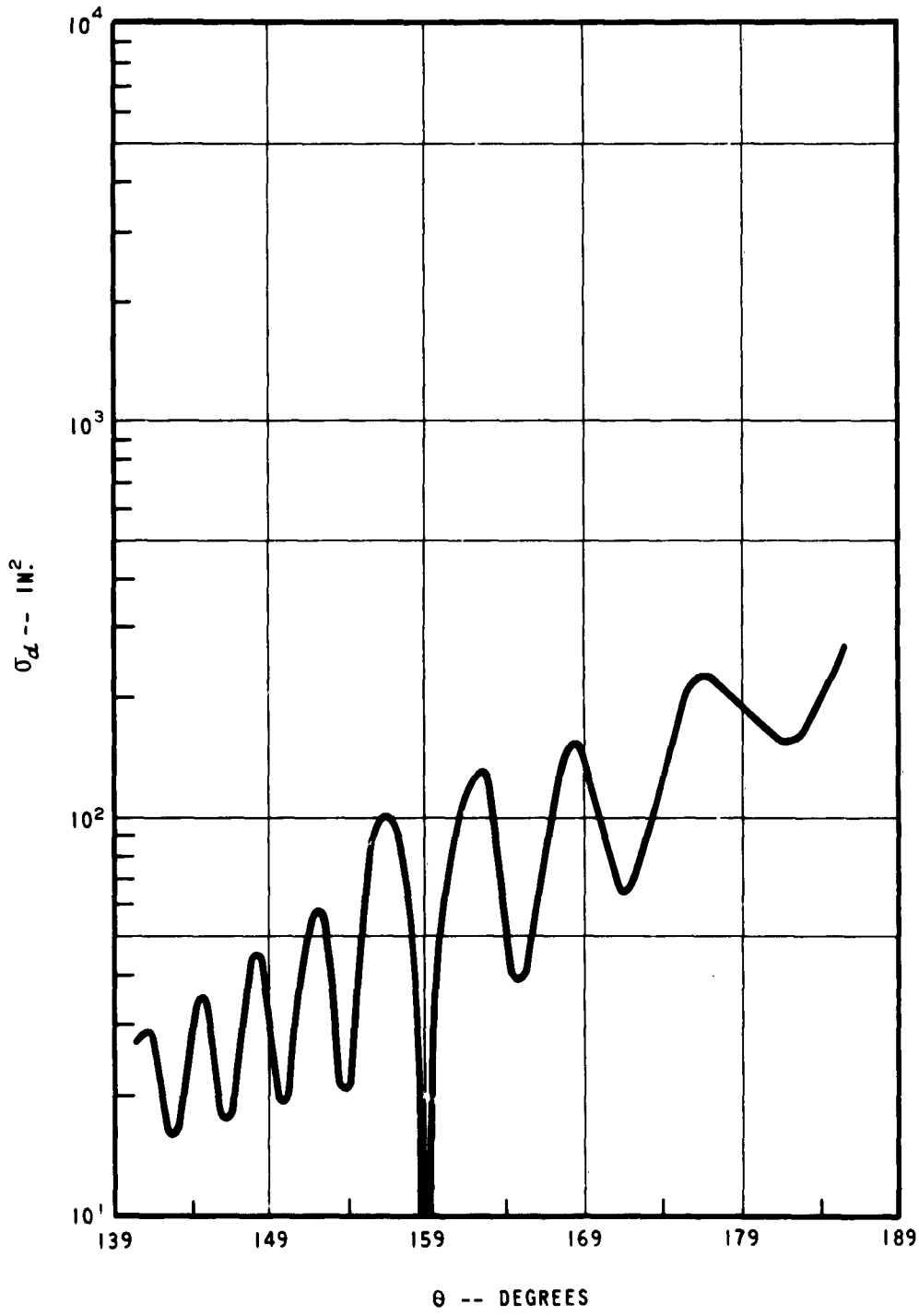

Figure 19. σ_d for $\theta_o = \pi - 42^o$ and $\varphi = 0, \pi$.

REFERENCES

1. V. A. Fock, "The Distribution of Currents by a Plane Wave on the Surface of a Conductor", Jour. of Phys. 10, 130-136, 1946. J. B. Keller, "A Geometrical Theory of Diffraction", Calculus of Variation and its Applications, Proc. of Symp. in Appl. Math. Vol. 8, 27-52 (McGraw-Hill Book Co., 1958). An elementary survey of approximation procedures is given in V. Twersky, "Electromagnetic Waves", Physics Today 13, 30-36 (1960). Recent developments are reviewed by L. B. Felsen and K. M. Siegel, "Diffraction and Scattering", J. Res. NBS 64D, 707-714 (1960).

2. K. M. Siegel, et al, "Studies in Radar Cross Sections VIII" (Willow Run Research Center, Ann Arbor, Michigan, 1953).

3. L. Mower and V. Twersky, "On Scattering of Electromagnetic Waves by Missile-Like Objects (U)", Report Confidential, EDL-E4, Sylvania Electronic Defense Laboratories; the cone is treated in the unclassified portion of the report.

4. P. M. Morse and H. Feshbach, "Methods of Theoretical Physics" (McGraw-Hill Book Co., 1949), 1380 ff and 1551 ff.

5. S. Silver, "Microwave Antenna Theory and Design" (McGraw Hill Book Co., 1949).

6. K. M. Siegel, Appl. Sci. Res. B7 (1959) 293.

7. K. M. Siegel, R. F. Goodrich and V. H. Weston, Appl. Sci. Res. B8 (1959).

8. J. B. Keller, "Back Scattering from a Finite Cone", New York University, Institute of Mathematical Sciences, Division of Electromagnetic Research, Research Report No. EM-127, 1959.

9. J. E. Burke and J. B. Keller, "Diffraction by Finite Bodies of Revolution", Report EDL-E49, Sylvania Electronic Defense Laboratories, 1960.

10. R. C. Bartle, C. I. Beard, J. E. Burke, M. E. Juza, and V. Twersky, "Optical Scattering Range, and Studies on Simple Shapes", Report EDL-M258, Sylvania Electronic Defense Laboratories, 1960.

11. V. Twersky, "On a New Class of Boundary Value Problems of the Wave Equation", Report EDL-E32, Sylvania Electronic Defense Laboratories, 1958.

AD ______ Accession No. ______
Electronic Defense Labs., Mountain View, Calif.
ELEMENTARY RESULTS FOR HIGH FREQUENCY SCATTERING BY CONES - J. E. Burke, L. Mower, and V. Twersky. Engineering Report EDL-E58, 24 April 1961 (Contract DA 36-039 SC-87475) UNCLASSIFIED Report.

Elementary high frequency results for scattering by finite cones are obtained by approximating the surface fields in the integral representation by their geometrical optics values. Both singly and doubly truncated cones are considered. A general expression is obtained for the location of the "Specular beam" (i.e., the surface generated by the geometrically reflected rays), and simple results for the field on and off the "beam" are developed. In particular, it is shown that for many practical purposes a universal curve exists for the scattering pattern. This curve, which depends on a parameter involving the cone's length and half angle, falls more or less between the Fraunhofer "aperture" patterns for the strip and disk, and differs essentially in that the minima are not zero. Numerical illustrations are given.

UNCLASSIFIED Copy No.

1. Aperture
2. Beam
3. Cones
4. Curves
5. Electromagnetic (Fields)
6. Fields
7. Finite
8. Geometry
9. High frequency
10. Integrals
11. Pattern
12. Representations
13. Scalar
14. Scattering
15. Specular
16. Truncated

I. Burke, J. E.
II. Mower, L.
III. Twersky, V.
IV. Contract DA 36-039 SC-87475

8. 5: 15. 1

AD ______ Accession No. ______
Electronic Defense Labs., Mountain View, Calif.
ELEMENTARY RESULTS FOR HIGH FREQUENCY SCATTERING BY CONES - J. E. Burke, L. Mower, and V. Twersky. Engineering Report EDL-E58, 24 April 1961 (Contract DA 36-039 SC-87475) UNCLASSIFIED Report.

Elementary high frequency results for scattering by finite cones are obtained by approximating the surface fields in the integral representation by their geometrical optics values. Both singly and doubly truncated cones are considered. A general expression is obtained for the location of the "Specular beam" (i.e., the surface generated by the geometrically reflected rays), and simple results for the field on and off the "beam" are developed. In particular, it is shown that for many practical purposes a universal curve exists for the scattering pattern. This curve, which depends on a parameter involving the cone's length and half angle, falls more or less between the Fraunhofer "aperture" patterns for the strip and disk, and differs essentially in that the minima are not zero. Numerical illustrations are given.

UNCLASSIFIED Copy No.

1. Aperture
2. Beam
3. Cones
4. Curves
5. Electromagnetic (Fields)
6. Fields
7. Finite
8. Geometry
9. High frequency
10. Integrals
11. Pattern
12. Representations
13. Scalar
14. Scattering
15. Specular
16. Truncated

I. Burke, J. E.
II. Mower, L.
III. Twersky, V.
IV. Contract DA 36-039 SC-87475

8. 5: 15. 1

AD ______ Accession No. ______
Electronic Defense Labs., Mountain View, Calif.
ELEMENTARY RESULTS FOR HIGH FREQUENCY SCATTERING BY CONES - J. E. Burke, L. Mower, and V. Twersky. Engineering Report EDL-E58, 24 April 1961 (Contract DA 36-039 SC-87475) UNCLASSIFIED Report.

Elementary high frequency results for scattering by finite cones are obtained by approximating the surface fields in the integral representation by their geometrical optics values. Both singly and doubly truncated cones are considered. A general expression is obtained for the location of the "Specular beam" (i.e., the surface generated by the geometrically reflected rays), and simple results for the field on and off the "beam" are developed. In particular, it is shown that for many practical purposes a universal curve exists for the scattering pattern. This curve, which depends on a parameter involving the cone's length and half angle, falls more or less between the Fraunhofer "aperture" patterns for the strip and disk, and differs essentially in that the minima are not zero. Numerical illustrations are given.

UNCLASSIFIED Copy No.

1. Aperture
2. Beam
3. Cones
4. Curves
5. Electromagnetic (Fields)
6. Fields
7. Finite
8. Geometry
9. High frequency
10. Integrals
11. Pattern
12. Representations
13. Scalar
14. Scattering
15. Specular
16. Truncated

I. Burke, J. E.
II. Mower, L.
III. Twersky, V.
IV. Contract DA 36-039 SC-87475

8. 5: 15. 1

AD ______ Accession No. ______
Electronic Defense Labs., Mountain View, Calif.
ELEMENTARY RESULTS FOR HIGH FREQUENCY SCATTERING BY CONES - J. E. Burke, L. Mower, and V. Twersky. Engineering Report EDL-E58, 24 April 1961 (Contract DA 36-039 SC-87475) UNCLASSIFIED Report.

Elementary high frequency results for scattering by finite cones are obtained by approximating the surface fields in the integral representation by their geometrical optics values. Both singly and doubly truncated cones are considered. A general expression is obtained for the location of the "Specular beam" (i.e., the surface generated by the geometrically reflected rays), and simple results for the field on and off the "beam" are developed. In particular, it is shown that for many practical purposes a universal curve exists for the scattering pattern. This curve, which depends on a parameter involving the cone's length and half angle, falls more or less between the Fraunhofer "aperture" patterns for the strip and disk, and differs essentially in that the minima are not zero. Numerical illustrations are given.

UNCLASSIFIED Copy No.

1. Aperture
2. Beam
3. Cones
4. Curves
5. Electromagnetic (Fields)
6. Fields
7. Finite
8. Geometry
9. High frequency
10. Integrals
11. Pattern
12. Representations
13. Scalar
14. Scattering
15. Specular
16. Truncated

I. Burke, J. E.
II. Mower, L.
III. Twersky, V.
IV. Contract DA 36-039 SC-87475

8. 5: 15. 1